The induction of SHP-1 degradation by TAOK3 ensures the responsiveness of T cells to TCR stimulation

Alexandre Poirier[1,2], João Vitor Silva Ormonde[3], Isabelle Aubry[1,4], Belma Melda Abidin[1], Chu-Han Feng[1,5], Zuzet Martinez-Cordova[1,5], Ana Maria Hincapie[1,4], Chenyue Wu[5], Luis Alberto Perez Quintero[1], Chia-Lin Wang[6], Anne Claude Gingras[7,8], Joaquín Madrenas[9], Michel L. Tremblay[1,4,10*]

[1]Goodman Cancer Institute, McGill University, Montréal, H3A 1A3, Québec, Canada. [2]Department of Experimental Medicine, McGill University, Montréal, Québec, Canada. [3]Brazilian Biosciences National Laboratory, Center for Research in Energy and Materials (LNBio – CNPEM), Campinas, São Paulo, Brazil. [4]Department of Biochemistry, McGill University, Montréal, Québec, Canada. [5]Department of Microbiology and Immunology, McGill University, Montréal, Québec, Canada. [6]NYU Langone Medical Center, 660 1st Ave, Fl 5, New York City, New York 10016, USA. [7]Lunenfeld-Tanenbaum Research Institute, Mount Sinai Hospital, Toronto, Canada. [8]Department of Molecular Genetics, University of Toronto, Toronto, Canada. [9]Department of Medicine, David Geffen School of Medicine at UCLA, Los Angeles, CA 40095, USA. [10]Faculty of Medicine, McGill University, Montréal, Québec, Canada.

*Corresponding author. Email: michel.tremblay@mcgill.ca

Abstract

Thousand-and-one-amino-acid kinase 3 (TAOK3) is a serine and threonine kinase that belongs to the STE-20 family of kinases. Its absence reduces T cell receptor (TCR) signaling and increases the interaction of the tyrosine phosphatase SHP-1 with the kinase LCK, a key downstream mediator of TCR signaling. Herein, we further investigated the mechanism by which TAOK3 limits the interaction of SHP-1 with LCK, using mouse models and human cell lines. The loss of TAOK3 decreased the survival of naïve $CD4^+$ T cells by dampening the transmission of tonic and activation-induced TCR signaling, respectively. In mouse T cells, Taok3 promoted the secretion of interleukin-2 (IL-2) in response to TCR activation in a manner that depended on *Taok3's* gene dosage and its kinase activity. TCR desensitization in knockout T cells was

caused by an increased abundance of Shp-1, a major negative regulator of proximal TCR signaling. Pharmacological inhibition of Shp-1 rescued the activation potential of Taok3-deficient T cells. TAOK3 phosphorylated Thr^{394} in the phosphatase domain of SHP-1, which promoted its ubiquitylation and proteasomal degradation. The loss of TAOK3 had no effect on the abundance of SHP-2, which lacks a residue corresponding to SHP-1 Thr^{394}. Modulation of SHP-1 abundance by TAOK3 thus serves as a rheostat for TCR signaling and determines the activation threshold of T lymphocytes.

Introduction

Initiation of the T cell receptor (TCR) signaling pathway relies on binding of the TCR to an antigen-bound major histocompatibility complex. This stimulates numerous intracellular phosphorylation events that lead to the activation and proliferation of T cells. TCR signaling initially relies on the Src family kinase LCK, which is associated with the intracellular domain of the TCR coreceptor CD4, to phosphorylate the immunoreceptor tyrosine-based activation motifs (ITAMs) in the intracellular chains of the TCR complex (*1-3*). During these early stages of activation, several regulatory proteins maintain the balance between activation and homeostasis, most notably the protein tyrosine phosphatase SHP-1, which is one of the most critical negative regulators of proximal TCR signaling. SHP-1 dephosphorylates the TCR ITAMs and prevents their phosphorylation by directly inactivating LCK, and it also dephosphorylates the protein tyrosine kinase ZAP-70, which is recruited to phosphorylated ITAMs and necessary for subsequent steps TCR signaling (*4, 5*). For the most part, SHP-1 prevents signaling from reaching downstream protein kinases, such as the mitogen-

activated protein kinases (MAPKs) extracellular signal–regulated kinases 1 and 2 (ERK1/2), Jun N-terminal kinase (JNK), and p38. These kinases, in turn, promote the activation of several transcription factors, such as nuclear factor of activated T cells (NFAT) family proteins, activator protein-1 (AP-1), and nuclear factor κ-light-chain-enhancer of activated B cells (NF-κB) (*6, 7*). NFAT, AP-1, and NF-κB act in concert to orchestrate the production of interleukin-2 (IL-2), a cytokine that is a hallmark of T cell activation (*8*). IL-2 is primarily produced by $CD4^+$ T cells and guides the proliferation and differentiation of T cells into effector T-helper cells (*9, 10*).

Considerable effort has been put into identifying pathways that regulate the activation of T cells. One noteworthy example is the STE-20 family of kinases. STE-20 kinases participate in the Salvador-Warts-Hippo (SWH) pathway, which is known chiefly for controlling cell proliferation and apoptosis (*11*). In addition to controlling organ size, the SWH pathway is crucial for numerous T cell functions, such as IL-2 secretion, migration, immunological synapse formation, and T lymphocyte memory (*12-15*). Beyond the core enzymes of this pathway, which include the mammalian STE-20–like kinases 1 and 2 (MST1/2) and large tumor suppressor 1 and 2 (LATS1/2), several other serine and threonine kinases positively regulate the SWH pathway, such as mitogen-activated protein kinase kinase kinase kinases (MAP4Ks) and thousand-and-one amino acid kinases (TAOKs) (*16, 17*). The third member in the sub-family of TAOKs, TAOK3, directly phosphorylates MST1/2 and LATS1/2 (*17, 18*) and therefore acts as an essential regulator of the SWH pathway. TAOK3 was initially identified as an interactor of epidermal growth factor receptor (EGFR) kinase substrate 8 (EPS8) and has been

proposed to act as an intermediate linking specific G protein–coupled receptors (GPCRs) to the p38 MAPK pathway (*19, 20*).

TAOK3 is found at high abundance in blood leukocytes and lymphoid organs, such as the thymus and spleen, suggesting a specific role in the hematopoietic compartment (*21*). TAOK3 is also critical for the formation of marginal zone B cells in the spleen (*22*). Studies showed that the generation of splenic type 2 conventional dendritic cells (cDC2s) and the occurrence of house dust mite (HDM)-induced allergic asthma both involve the TAOK3 kinase (*23, 24*). TAOK3 also functions as a negative regulator of inflammation and proinflammatory responses in macrophages (*25*). The function of TAOK3 has also been investigated in Jurkat T lymphoblasts, in which its deletion alters antigen dependant, but not antigen independent TCR activation (*26*). In this previous investigation, it was found that in absence of TAOK3, SHP-1 shows increased interaction with LCK, which results in decreased proximal TCR signaling. To address how TAOK3 limits the interaction between SHP-1 to LCK, we explored the role of TAOK3 in T cell activation using various approaches such as CRISPR-inducible deletion, knockout models, and naïve T cell isolation. Taok3 knockout naïve $CD4^+$ mouse T cells proliferated less than did their wild-type counterparts upon TCR engagement due to a combination of a desensitized TCR and reduced IL-2 secretion. We identified key residues in human TAOK3 that contributed to the production of IL-2 and showed that the enzyme's kinase activity was essential. Further dissection of proximal TCR signaling revealed that desensitization was caused by increased SHP-1 protein abundance and phosphatase activity. Under normal conditions, TAOK3

phosphorylated SHP-1 on Thr^{394} to promote its ubiquitylation and proteasomal degradation. The absence of TAOK3 thus increased the protein stability and abundance of SHP-1. Our findings uncover a mechanism that guides the sensitivity of the TCR signaling cascade and, consequently, T cell function.

Results

Taok3-deficient mice have reduced naïve $CD4^+$ T cell abundance and survival

To better understand the role and function of TAOK3, we aligned its protein sequence with that of the human reference proteome. As expected, human TAOK3 shares high homology with TAOK1 and TAOK2 (73.6 and 62.5%, respectively). We also found that MST1 and MST2 share high sequence identity with TAOK3 in their serine-threonine kinase domain (Fig. 1A). Because MST1 is an essential modulator of naïve T activation (21), we decided to contrast the transcriptional changes resulting from its activation with data extracted from the Database of Immune Cell Expression, eQTLs, and Epigenomics (DICE) (22). In contrast to transcripts encoding MST1, which showed a marked increase in abundance upon T cell activation, transcripts encoding TAOK3 decreased in both $CD4^+$ and $CD8^+$ activated human T cells, but more so in the latter (Fig. 1B). Among all the genes that were significantly decreased in expression after T cell activation, *TAOK3* ranked at the 60^{th} and 52^{nd} percentiles in $CD4^+$ and $CD8^+$ T cells, respectively (Fig. 1B). Activated naïve $CD4^+$ T cells had a marked decrease in *TAOK3* transcript abundance when compared to the other $CD4^+$ subsets (fig. S1A). To further elucidate the role of TAOK3 in T cells, we performed analyses of the spleens of full-body knockout (*Taok3*$^{-/-}$) mice. *Taok3*$^{-/-}$ mice were viable and fertile, had average weight, and displayed no

apparent phenotype. Flow cytometric analyses revealed a lower proportion and number of splenic $CD3^+$ cells (Fig. 1, C and D). This decrease was found for the $CD4^+$ and $CD8^+$ compartments without affecting the $CD4^+/CD8^+$ T cell ratio (Fig. 1, E to G). We thus pursued our analyses in the $CD4^+$ compartment, given that *TAOK3* ranked significantly higher in CD4+ cells than CD8+ cells (Fig. 1B).

We next sought to further investigate mature T cell populations in the periphery. Within the $CD4^+$ T cell population from *Taok3*-knockout compared with wild-type mice, we observed a lower percentage of naïve (T_n) cells and a higher percentage of effector (T_{EM}) and central memory (T_{CM}) subsets (Fig. 1H). This abnormal distribution resulted in an approximately 50% decrease in $CD4^+$ naïve T cell numbers (Fig. 1, H and I). There were no changes in the proportion of $FOXP3^+CD25^+CD4^+$ regulatory T (T_{reg}) cells (fig. S1, B and C). To further explore whether the secretory function of CD4+ cells was intact in Taok3-deficient mice, we quantified cytokine amounts by cytokine multiplexing. Serum type II interferon (IFN-γ) concentrations remained unchanged, whereas IL-2 abundance was decreased by 64% (Fig. 1J). The relative amounts of the T cell–supporting cytokines IL-7 and IL-15 remained unchanged (fig. S1D). Flow cytometric analyses of axillary and inguinal lymph nodes and bone marrow also revealed decreased $CD4^+$ T cell numbers, as was observed in the spleen (fig. S1, E to H). Finally, we found greater frequencies of apoptotic naïve, central memory, and effector memory $CD4^+$ T cells in both spleens and lymph nodes (Fig. 1K, fig. S1I). Naïve T cells were also found to have a decreased amounts of Nur77, a marker of tonic TCR signaling in homeostatic conditions (Fig. 1L and fig. S1J). Altogether, these

observations suggest that Taok3 plays a vital role in $CD4^+$ naïve T cell homeostasis, survival, and in maintaining IL-2 abundance in the blood.

Taok3 is required for TCR sensitivity in naïve $CD4^+$ T cells

To better understand whether the above phenotypes were linked to TCR function, we performed proliferation analyses on isolated naïve $CD4^+$ mouse T cells in vitro (fig. S2, A and B). To mimic partial and complete TCR agonists, we used two concentrations of CD3-specific antibody plus IL-2: 2µg/mL antibody + 20U/mL IL-2 for partial TCR activation and 10µg/mL antibody ± 20 U/ML IL-2 for complete TCR activation. Carboxyfluorescein-succinimidyl-ester (CFSE) analyses revealed a significant difference in the distributions of daughter generations issued from the activation of *Taok3*$^{-/-}$ naïve $CD4^+$ T cells after 72h. At 2µg/mL of CD3-specific antibody, a significant proportion of T cells failed to engage in proliferation, and those that did failed to proliferate as well as their wild-type counterparts (Fig. 2, A and B). Analysis of the abundance of CD69, an early cell surface marker of T cell activation, potentially indicated a considerable reduction in the speed of activation of those cells (Fig. 2C). Further experimentation at an earlier time point (48h) corroborated this observation (fig. S2C). Increasing the concentration of CD3-specific antibody to 10µg/mL largely, but not completely, restored the proliferation of *Taok3*$^{-/-}$ naïve T cells (Fig. 2, D and E). The addition of exogenous IL-2 (20U/mL) was required to fully restore activation-induced proliferation (Fig. 2, D and E). The addition of IL-2 also abrogated the differences in CD69 abundance on cells that had divided three or more times (Fig. 2F). Taok3-deficient naïve $CD4^+$ T cells produced less IL-2 upon TCR engagement than did their

wild-type and heterozygous counterparts (Fig. 2G). TCR stimulation without the addition of exogenous IL-2 also led to decreased abundance of the IL-2 receptor IL-2Rα (CD25), another marker of T cell activation (Fig. 2H). To further examine the relationship between Taok3 and IL-2 secretion, we quantified the supernatants of total $CD4^+$ T cell suspensions stimulated with a gradient of CD3-specific (0, 0.25, 0.5, 1, 2,5 10, and 20 µg/mL) and CD28-specific (5µg/mL) antibodies for 24 hours. Using IL-2 ELISAs, we observed a dose-response relationship between *Taok3* expression and IL-2 secretion (Fig. 2I). Given that IL-2 is a critical landmark in the activation program of $CD4^+$ T cells, these results indicate that Taok3 is essential to maintain the sensitivity of the TCR to activation in naïve $CD4^+$ T cells. The secretion of granulocyte-macrophage colony-stimulating factor (GM-CSF) and IL-10 was also increased after 24 hours of CD3 and CD28 stimulation, whilst IFN-γ and tumor necrosis factor (TNF) was not (fig. S2D). Altogether, these results indicate that Taok3 is crucial for the sensitivity of the TCR. We thus propose that Taok3 sensitizes the TCR activation threshold in naïve $CD4^+$ T cells.

TAOK3 substitution mutants control the production of IL-2 upon TCR engagement

To further refine the enzyme's role in T cell activation, we studied the effect of point mutations affecting human TAOK3 on both IL-2 production and proliferation. Lentiviral vectors encoding V5-tagged wild-type human TAOK3 (TAOK3-V5) were constructed in parallel with the V5-tagged single substitution mutants Y256F, Y305F, and S324A and the double substitution mutant T181A Y183F (T181A/Y183F) (Fig. 3A). Among these mutants, only S324A has been previously reported to have a functional impact, with TAOK3 S324A failing to activate the P38 pathway during cellular stress responses (*27*).

We investigated the other mutants because they have been highlighted as frequent phosphorylation sites in *phosphoSitePlus* (*28*). The lentiviral particles were used to transduce the previously described TAOK3 knockout Jurkat T cells to test for rescue in the knockout background (*26*)(Fig. 3B). We first assessed the steady-state growth rate of the various mutant cell lines with live cell imaging to monitor confluence of the cultures (Fig. 3C). Expression of the mutants TAOK3-Y256F-V5 and TAOK3-S324A-V5 resulted in reduced proliferation compared to the expression of TAOK3-V5, but expression of kinase-deficient TAOK3-T181A-Y183F-V5, a mutant lacking the phosphorylatable Thr-X-Tyr motif in the MAPK activation loop (*29*), increased proliferation (Fig. 3C). The almost identical abundances of CD3 and CD28 across the cell lines indicated a similar potential for activation with CD3- and CD28-specific antibodies for all cell lines (Fig. 3D). Rescue with TAOK3-V5 enhanced the IL-2 production of KO cells by about 1-fold in response to TCR signaling (Fig. 3E). This result indicates consistency in the modulatory effect of TAOK3 and IL-2 production because both the genetic deletion (in vivo serum and in vitro stimulated) and rescue had a +/- 1-fold effect. The expression of mutants TAOK3-Y256F-V5 and TAOK3-S324A-V5 further enhanced the IL-2 response (Fig. 3E), which possibly indicates that under normal circumstances, phosphorylation of those residues reduces the activity of TAOK3. To independently assess the role of the enzyme's catalytic activity on IL-2 secretion, we stimulated wild-type murine $CD4^+$ T cells for 24 hours with Compound-43, a TAO-kinase inhibitor (*30*). Concentrations of 3 and 10μM significantly decreased IL-2 production (Fig. 3F). Finally, we investigated the role of TAOK3 in the activation of several MAPKs such as JNK, P38, and ERK (fig. S3, A to C). Transfection of TAOK3

mutants into HEK293T/17 cells revealed that both the Y256F and S324A mutants increased JNK, but not P38, phosphorylation compared to wild-type TAOK3 (fig. S3A). TCR-stimulated $CD4^+$ T cells also showed decreased JNK, ERK, and NF-κB p65 phosphorylation (fig. S3, B to E). These findings indicate that amino acid substitutions in TAOK3's regulatory serine rich region can increaseTCR induced IL-2 secretion and JNK signaling.

An increase in SShp-1abundance and activity limits TCR signaling strength in Taok3-deficient T cells

We wondered whether the decrease in TCR sensitivity observed in naïve $CD4^+$ T cells could be due to signaling defects happening during the initial stages of TCR activation, before the activation of MAPKs, such as JNK .. TCR signaling is first initiated by the phosphorylation of Lck at Tyr^{394} which activates the kinase (*31*). In a similar fashion, ZAP-70 Tyr^{319} phosphorylation is necessary for the propagation of TCR signaling (*32*) . We observed both decreased Lck Tyr^{394} and Zap-70 Tyr^{319} phosphorylation in wild-type versus Taok3-deficient murine T cells (Fig. 4A and fig. S4A). Further investigations revealed a decreased intensity of calcium influx upon CD3 stimulation in Taok3-deficient naïve $CD4^+$ T cells compared to wild type (Fig. 4B). These patterns of impaired proximal signaling were consistent with the involvement of Shp-1, given that it dephosphorylates Lck Tyr^{394} and ZAP-70 Tyr^{319} (*33*). We thus assessed whether the deletion of *Taok3* affected Shp-1

abundance and activity. An increase in Shp-1 protein abundance of about 0.8-fold in $Taok3^{+/-}$ and 3-fold in $Taok3^{-/-}$ was observed in $CD4^+$ T cells (Fig. 4C). No differences in

the abundance of transcripts encoding Shp-1 (*Ptpn6*) were detected between genotypes, suggesting that the mechanism behind the increase in Shp-1 protein is posttranslational in nature (Fig. 4D). Quantification of Shp-1 protein abundance in both $CD4^+$ T cells and CD4-depleted splenocytes showed that increased abundance was found in $CD4^+$ T cells but not total splenocytes (Fig. 4E and fig. S4B). We next quantified Lck Tyr^{505} phosphorylation to independently determine the activation status of Lck and thus, proximal TCR signaling in isolated naïve $CD4^+$ T cells (Fig 4F). Under normal circumstances, Tyr^{505} is phosphorylated to decrease the activity of Lck after TCR engagement (*34*). Phosphorylation of Lck at Tyr^{505} was significantly higher in resting *Taok3*$^{-/-}$ cells and remained unchanged throughout the different time points of TCR stimulation, unlike wild-type cells, which were responsive to CD3 stimulation (Fig. 4F and fig. S4C).

To examine whether the catalytic activity of SHP-1 was responsible for the decreased TCR activation threshold, we stimulated naïve $CD4^+$ T cells with 5μg/mL of CD3 and CD28 antibodies and added different concentrations of NSC-87877, a SHP-1 and SHP-2 inhibitor (*35*). Pharmacological inhibition rescued the frequency of activated $CD25^+$ cells, IL-2 production, and the frequency of $Nur77^+$ cells but not CD69 expression (Fig. 4G and fig. S4D). To validate those findings in a T cell–specific loss-of-function model, we generated an inducible CRISPR *Taok3* deletion mouse model. Expression of the Cas-9 enzyme was under the control of the Cre-recombinase inserted into the *CD4* locus (Fig. 4H and fig. S4E). Unfortunately, inducible deletion could not be achieved in vivo. We therefore isolated splenic T cells from these mice and induced *Taok3* deletion ex vivo. We observed that *Taok3*-deleted T cells had increased proliferation but also

higher abundance of cleaved caspase-3 in IL-7–containing culture medium, indicating higher cellular turnover (fig. S4, F to H). In *Taok3*-deleted T cells, Shp-1 protein was increased and was accompanied by decreased phosphorylation of Lck Tyr^{394}, Mek1/2 $Ser^{217/221}$, and Erk Thr^{202}/Tyr^{204} and increased phosphorylation of Lck Tyr^{505}, validating previous observations (Fig 4I and fig. S4I). Stimulation-induced IL-2 production was lower in *Taok3*-deleted cells compared to control cells after 96h of stimulation (Fig. 4J). Deletion also reduced the abundance of IL-2Rα (CD25) and IL-2Rβ (CD122) after 24h of stimulation (Fig 4K). These results from independent models (T cells from *Taok3* whole-body knockout mice and T cells in which *Taok3* knockout was induced ex vivo) agree in demonstrating that Shp-1 protein overexpression is the main driver behind TCR desensitization absence of Taok3.

TAOK3 preferentially interacts with the active form of SHP-1 and directly phosphorylates Thr^{394} in the catalytic domain

To explore the posttranslational mechanism behind the Shp-1 overabundance in Taok3-deficient T cells, we first sought to determine if human TAOK3 and SHP-1 interacted with one another. We first co-transfected FLAG-tagged SHP-1 (FLAG-SHP-1) and human-TAOK3 with or without the constitutively active Y527F SRC kinase mutant (Fig. 5A). HEK293T/17 cells lack the appropriate TCR machinery that would normally provide with high levels of protein phosphorylation, which are often necessary for protein-protein interactions to occur. SRC Y527F was thus used to increase Tyrosine phosphorylation of signaling molecules, as would be the case during TCR signaling. In this system, SHP-1 is phosphorylated at Tyr^{536} by SRC Y527F, which promotes protein-protein and

substrate-protein interactions to occur, as it would be the case during TCR engagement. Constitutively active SRC also phosphorylates several substrates that would normally trigger the activation and proliferation of T cells, such as phospholipase C γ1 (PLCγ1), phosphoinositide 3-kinase (PI3K), and Erk1/2 (*36, 37*). SHP-1 coimmunoprecipitated with TAOK3, and the presence of SRC Y527F further increased SHP-1 coimmunoprecipitation (Fig. 5A). We validated the reciprocity of this interaction by immunoprecipitating SHP-1 (Fig. 5B). We also performed FLAG-SHP-1 immuoprecipitation using the phosphatase trapping mutants C453S or D419A to investigate whether TAOK3 was a substrate of SHP-1 (Fig. 5B). The mutated C/S or D/A variants markedly enhance the affinity between a protein tyrosine phosphatase and its substrate (*38, 39*). No substrate-trapping effect was observed with the mutated variants, implying that TAOK3 is likely not a direct substrate of SHP-1 (Fig. 5B). Pulldown assays using purified recombinant GST-tagged proteins provided additional evidence for direct interaction between SHP-1 and TAOK3 (fig. S5, A and B). To validate the occurrence of this interaction between endogenous proteins in the context of T cell signaling, we performed TAOK3 immunoprecipitation in resting (0), or 15-minute stimulated (15) Jurkat T cells. SHP-1 coimmunoprecipitated with TAOK3 only when the TCR signaling cascade was engaged and not under resting conditions (Fig. 5C).

To define the region of interaction between TAOK3 and SHP-1, we cotransfected HEK293T cells with SHP- 1 truncation mutants (Fig. 5D), wild-type TAOK3, and SRC Y527F. The ΔC72 form of SHP-1, which lacks the last 72 amino acids of the C-terminus, was not immunoprecipitated by TAOK3 (Fig. 5E and fig. S5C). Conversely, we

observed increased coimmunoprecipitation of the ΔN-SH2, C-SH2 mutant form of SHP-1, which has increased catalytic activity due to loss of the N-SH2, C-SH2 self-regulatory domains, suggesting that TAOK3 has greater affinity for the active form of SHP-1 (Fig. 5E and fig. S5C). This result is consistent with our finding that the presence of SRC Y527F, which promotes the activation of SHP-1 catalytic activity by phosphorylating SHP-1 at Tyr^{536}, increased SHP-1 coimmunoprecipitation with TAOK3 (Fig. 5A). We also tested whether SHP-1 was a substrate of TAOK3 in in vitro kinase assays. Purified FLAG-SHP-1 proteins were incubated with or without the kinase domain of TAOK3 (Fig. 5F and fig. S5D). Reactions were analyzed by mass spectrometry to detect phosphorylated residues. We discovered that TAOK3 phosphorylated SHP-1 on Thr^{394}, a residue located in the catalytic domain of the phosphatase (Fig. 5F). We modelized the SHP-1 phospho-Thr^{394} and TAOK3 complex using available Alpha Fold structures and HADDOCK 2.4 (Fig. 5G). Overall, our results indicated that SHP-1 is a direct target of TAOK3 and that the two enzymes from a complex that requires the C-terminal tail of SHP-1 for interaction.

TAOK3 promotes the ubiquitylation and proteasomal degradation of SHP-1

To understand the biological relevance of the TAOK3-SHP-1 interaction and to test whether TAOK3 disrupted the crosstalk between SRC and SHP-1, we performed affinity-capture mass spectrometry (AP-MS) using SHP-1 as bait. We quantified SHP-1–interacting proteins in HEK293T/17 cells into which FLAG-SHP-1 was cotransfected with either TAOK3 or SRC Y527F or both. Analysis of the protein abundance profiles revealed distinct enrichment profiles for the different transfection conditions (Fig. 6, A

and B). TAOK3 induced both the enrichment and the decrease of SHP-1 protein-protein interactions (Fig. 6B). SIRT1, DDX39B, BCR, and MARK2 were amongst the most significantly enriched proteins when TAOK3 was cotransfected with SHP-1 (Fig. 6B). Conversely, the cotransfection of TAOK3 decreased the interactions between SHP-1 and ENO1, RAN, PRDX2, and SPTAN1. We next performed protein-interaction network analysis using GENEMANIA to identify key enriched and diminished protein interactions and functions (Fig. 6C) (*40*). We found that TAOK3 significantly disrupted the interaction between SHP-1 and proteins linked to metabolic activity (Fig. 6D). On the other hand, TAOK3 expression provoked an increase in interaction with proteins involved in DNA conformation change, gene silencing, regulation of gene expression, and RNA transport (Fig. 6D). In cells cotransfected with SRC Y527F, the addition of TAOK3 only changed the enrichment of two other proteins namely CAD and SMU1 (fig. S6B). These results suggest that TAOK3 significantly alters the interactome of SHP-1. Beyond that role, we found the enrichment of ubiquitin E3 ligases such as RAD18 (Fig. 6B and fig. S6A). Given that TAOK3 increased the interaction of SHP-1 with ubiquitin E3 ligases, in the SHP-1 interactome, it was logical to determine whether TAOK3 instigated the degradation of SHP-1, an activity that was also consistent with previous evidence (Fig. 4C). To test that hypothesis, we created a doxycycline-inducible TAOK3 overexpression Jurkat cell line. Upon treatment with doxycycline, these cells overexpressed TAOK3 and had a marked decrease in SHP-1 protein abundance, suggesting degradation or destabilization of SHP-1 (Fig. 6E and fig. S6C). To determine if this phenomenon was the result of ubiquitin-mediated proteasomal degradation, we cotransfected HEK293T/17 cells with HA-tagged ubiquitin and FLAG-SHP-1 with or without TAOK3.

Cotransfection of TAOK3 led to the monoubiquitylation of SHP-1, as marked by an 8 kDa shift in the SHP-1 molecular weight (Fig. 6F). The addition of MG-132, a potent inhibitor of the 26S-proteasome (*41*), increased basal SHP-1 ubiquitylation and enabled the detection of polyubiquitylated SHP-1 in the TAOK3-expressing condition (Fig. 6F). Further experimentation with the non-phosphorylatable SHP-1 T394A mutant and the phospho-mimetic T394D mutant helped elucidate the role of Thr^{394} phosphorylation in this phenotype. We found that TAOK3-induced polyubiquitylation was lost in the T/A mutation (Fig. 6G). Conversely, SHP-1 T/D mutant had higher polyubiquitylation status with or without TAOK3 cotransfection (Fig 6G). Additional investigation revealed that Thr^{394} is not conserved in SHP-2, in which the corresponding position is occupied by glutamic acid (Glu^{400}), and that SHP-2 protein abundance remained unchanged between wild-type and *Taok3* knockout murine $CD4^+$ T cells (fig. S6, D and E). Further experimentation with CD3- and CD28-stimulated Jurkat cells revealed that SHP-1 had increased stability in TAOK3-deficient cells compared to wild-type upon treatment with cycloheximide (CHX) for 24h (Fig. 6H and fig. S6F). In contrast, SHP-2 stability remained unaffected by CHX treatment, regardless of stimulation (Fig. 6H and fig. S6F). These results demonstrate that TAOK3 promotes SHP-1 mono- and polyubiquitylation through Thr^{394} phosphorylation, leading to the proteasomal degradation of the phosphatase. TAOK3-induced, phosphorylation-mediated degradation was restricted to SHP-1 and did not affect SHP-2.

Discussion

SHP-1 is a major modulator of T lymphocyte activity through its negative regulation of the TCR and its role in the signaling of checkpoint receptors, such as PD-1 (*4, 42, 43*). Our identification of TAOK3-mediated SHP-1 phosphorylation and subsequent degradation represents a previously uncharacterized mechanism by which the intensity of TCR signaling is modulated. Our results also suggest the involvement of E3 ubiquitin ligases, such as RAD18, in the promotion of SHP-1 degradation, given the patterns of SHP-1 polyubiquitination. Several E3 ligases have already been identified as inducers of SHP-1 degradation, including RNF6, RNF38, SMURF1, Itch, and WWP2 (*44-47*). These ubiquitin ligases are all expressed in T cells and could mediate ubiquitylation of SHP-1- upon Thr^{394} phosphorylation. Our data also suggest that the endogenous SHP-1-TAOK3 interaction might preferentially form under specific conditions, such as during TCR engagement or Src-familly kinase activity.

In addition to promoting SHP-1 degradation, the ubiquitylation of SHP-1 decreases its association with Lck (*47*) and might therefore also serve as a positive feedback mechanism to sensitize proximal TCR signaling. Other phosphatases are also known to dephosphorylate Lck, namely PTPN22, PTPN2, and DUSP22 (*48-51*). However, it is unlikely that TAOK3 also targets those phosphatases given their lack of the consensus TAO kinase phosphorylation motif (*52, 53*). *Taok3*$^{-/-}$ T cells also phenocopy SHP-1–overexpressing transgenic (*ptpn6-tg*) T cells, with decreased TCR signaling (*54, 55*). Conversely, the deletion of SHP-1 does not impact T cell activation or development (*56*). This might imply that T cells can compensate for SHP-1 loss more easily than for SHP-1 increase, perhaps through the functional redundancy of other phosphatases such as SHP-2, PTPN2, and/or PTPN22.

Independently of its activity on SHP-1, TAOK3 promotes JNK phosphorylation, which would also promote IL-2 secretion by T cells through the activation of the Jun constituent of the dimeric AP-1 transcription factor, a heterodimer of Fos and Jun proteins (*57, 58*). Mutation of residues Tyr^{256} and Ser^{324} downstream of the kinase domain of TAOK3 markedly enhanced the activation of JNK and the production of IL-2. These results suggest that under normal circumstances, phosphorylation of these residues reduces the function of TAOK3. These residues may contribute to conformational autoinhibition of the kinase domain of TAOK3, which could be mediated by disordered serine-rich or coiled-coiled domains, not unlike that described for other STE-20 kinases (*59, 60*). TAOK3 also has the potential to form protein-protein interactions through these other domains. A study by Bagci *et al*. (*61*) showed that TAOK3 interacts with the Rho GTPase RAC1. Although the exact regions of interaction between the two proteins remains unknown, it is likely that that interaction involves the coiled-coiled domain of TAOK3. This interaction could also participate in TCR signaling dynamics independently of SHP-1 (*62, 63*). Given that TAOK3 phosphorylates Thr^{394} in the protein tyrosine phosphatase (PTP) domain of SHP-1, but that the C-terminal tail was also found to be important for binding, it is possible that TAOK3 docks onto the C-terminal tail of SHP-1 through its coiled-coiled domain. Docking could then induce conformational changes in TAOK3 that enable binding to the target region. This hypothesis remains to be validated.

Here, we also demonstrated that increasing TCR stimulation not only rescued the proliferative capacity of TAOK3-deficient, naïve T cells, but also that newly formed cells exhibited more pronounced effector-like phenotypes. The role of IL-10 in the promotion

of effector cell differentiation remains conflicted, but in our hands, IL-10 abundance correlated with increased memory-like cell formation in *Taok3* knockout T cells (*64*). These observations imply that TAOK3 exerts a differential role in naïve versus memory-like T cells. A possible explanation for this is that naïve T cells use the ERK1/2, p38, and JNK pathways differently to how they are used by effector-memory cells (*65-67*). Our group and others have demonstrated the capacity of TAOK3 to promote JNK signaling (*68*). These reports conflict with initial studies that reported TAOK3 as being inhibitory toward JNK, hence its initial name “JNK-inhibitory kinase (JIK)” (*69*). The most likely scenario is that the ability of TAOK3 to phosphorylate JNK is cell type–specific. Indeed, TAOK3 was reported as a positive regulator of JNK phosphorylation in Jurkat E6.1 (T cells), HEK293T/17 (kidney origin), immortalized hepatocytes (*68*), and osteoblasts (*70*). On the other hand, TAOK3 is a negative regulator of JNK phosphorylation in mouse brain cells (*71*), fibroblasts, and cervical cells (*69*). TAOK1 inhibits JNK signaling in HeLa cells (cervical cells) upon IL-17 stimulation (*72*).

Other STE-20 kinases are also considered as potent modulators of immune signaling through their activation of the ubiquitin-proteasome system (*73, 74*). Our studies thus point to some redundancy between TAOKs and other STE-20 kinases. There is, however, functional divergence between some STE-20 kinases, such as MAP4K1 (also known as HPK1) (*75*) and MAP4K3 (also known as GLK) (*76*), which could be a consequence of different protein domain composition and substrate specificities (*52, 77*). Studies have also reported a link between TAOKs and NF-κB–mediated inflammation, tumorigenesis (*78-80*), and drug resistance (*81, 82*). Inhibitors of TAOK family kinases have shown some potential for cancer therapy (*30, 83, 84*). Our results

define additional potential functions for TAOK3 in cancer cells, such as DNA conformational change, regulation of gene expression, and RNA transport. Overall, we conclude that TAOK3 is important in the modulation of SHP-1 degradation through phosphorylation of Thr^{394} in the PTP domain of the phosphatase (Fig. 7). The absence of TAOK3-mediated degradation reduces TCR reactivity and T cell activation. Destabilization of SHP-1 thus serves as a mechanism to increase the reactivity of the TCR signaling cascade.

Materials and Methods

Mice

Whole-body Taok3 KO mice were purchased from Jackson laboratories MMRRC stock #43790. These mice were generated by the KOMP team using a CRISPR-generated KO mutant of the Taok3 kinase by deleting exon 6, leading to a frameshift mutation causing an early stop codon (*85*). *Taok3*$^{-/-}$ mice were bred with background-compatible CD57/Bl6 mating partners. Control animals for *Taok3*$^{-/-}$ mice were *Taok3*$^{+/+}$ littermates from the heterozygous breedings mentioned earlier. Animals were housed and bred in specific-pathogen-free facilities at the Comparative Medicine and Animal Resources Centre (CMARC) at McGill University in accordance with the Canadian Council on Animal Care Guidelines. The engineered mouse Embryonic Stem Cells (ESCs) were generated in collaboration with Mirimus Inc. (Brooklyn, NY). The Cas9D10A-IRES-tGFP cassette was synthesized and cloned into Col1A1-TRE-LSL-tGFP-miR30 backbone (*86*) to form the vector Col1A1-TRE-LSL-Cas9D10A-IRES-tGFP. *Taok3* exon 7 and exon 8 were identified to generate gene insertions and deletions (INDELs) (*87*). Three pairs of

small guide RNAs (sgRNAs) were designed targeting each of these exons and cloned upstream of the Tetracycline Responsive Element (TRE) into the Col1A1-TRE-LSL-Cas9D10AIRES-tGFP targeting vector. The *Taok3* sgRNA-containing targeting construct was electroporated into pre-engineered KH2 ESCs (Lonza 4D-NucleofectorTM System, Program CG-104) (*86*). These cells contain the reverse tet-transactivator (rtTA) driven by the endogenous Rosa26 locus (Rosa-rtTA). The construct was targeted downstream of the constitutively expressed *Col1A1* locus. The resulting off-frame exons are expected to be unable to code for proteins. Stable transfectants were selected through hygromycin selection and individually picked after one week. Individual colonies were transduced with Cre-encoding adenovirus and treated with doxycycline (Dox) (1 μg/ml) for 24 hours to assess Cas9 expression by Western blot and *Taok3* gene targeting by DNA sequencing. ESCs expressing the second pair of sgRNAs targeting exon 8 (exon 8-2) were selected for microinjection and generation of the mouse colony (Charles River Laboratories, Wilmington, MA). The sgRNA sequences were: sg*Taok*3-Exon8-2f: TCAGCCAGCTTCACCTGACCTGG and sg*Taok*3-Exon8-2b: CTCCCGCCAACTCCTTTGTGGGG. Validation of deletion of *Taok3* exon 8 with PCR using primers: Forward-CCGCTCGAGTCGCTAATTGCATGTTCTGG and Reverse-TATGAATTCATCCATCTGAGGCCAATCTG. Transgenic iCRISPR mice were bred with CD4-Cre expressing mice. iCRISPR-mediated knockdown of Taok3 required extended periods of Doxycycline treatment. Splenocytes were treated with Doxycycline (Sigma, D3072-1ML) for five days. After this period, we purified the T cells and cultured them

with Dox. for additional seven days in the presence of recombinant murine IL-7 at 50ng/mL (Preprotech, 217-17).

Cell lines and culture

Mouse spleens were aseptically collected and mashed through 40 µM cell strainers for collection of whole cell suspensions in mouse R10 medium (RPMI supplemented with non-essential amino acids, 10% heat-inactivated FBS, 1mM sodium pyruvate, 2 mM L-glutamine, 100 µg/ml penicillin/streptomycin, 10 mM HEPES pH 7.0 and 0.1% 2-mercaptoethanol). T cells were purified by negative selection using EasySep™ Mouse Naïve $CD4^+$ T Cell Isolation Kit (, Stemcell technologies, 19765) or EasySep™ Mouse CD4 Positive Selection Kit II (Stemcell technologies, 18952) and used directly for functional assays or cultured with doxycycline (iCRSPR model). For extended cultures (iCRSPR model), cells were maintained in medium containing 50 ng/ml mouse recombinant IL-7 (PeproTech, 217-17). Jurkat cells (clone E6.1) and HEK 293T cells were purchased from American Type Culture Collection. *TAOK3*-deficient cell line Jurkat T3-19 was previously generated (*26*) and served as the source for transduction and stable expression of TAOK3 mutants (V5, T181AY183F-V5, Y256F-V5, Y305F-V5, S324A-V5). For doxycycline-inducible TAOK3-V5 overexpression, TET-ON-TAOK3-V5 was transduced in the TAOK3-V5 cell line. Overexpression was induced with 1µg/mL of Doxycycline (Sigma Aldrich, D3072-1ML) for 24 hours. Suspension cells were cultured in RPMI 1640 medium (Hyclone) supplemented with non-essential amino acids, 10% heat-inactivated FBS, 1mM sodium pyruvate, 2 mM L-glutamine, 100 µg/ml penicillin/streptomycin, 10 mM HEPES pH 7.0. Cells were cultured at 37°C, 5% CO2,

and 95% relative humidity. HEK 293T adherent cells used for transfections were cultured in DMEM high glucose (Hyclone, SH30022FS) supplemented with 10% FBS 100 µg/ml penicillin/streptomycin at 37°C, 5% CO2, and 95% relative humidity. For SHP-1 stability experiments, Jurkat E.6 cells were incubated with 20µM of Cyclo heximide (Sigma Aldrich, 66-81-9) or with DMSO vehicle for 24 hours.

Western blotting analysis

Cells were washed twice using ice-cold PBS supplemented with 400µM Na_3VO_4 and 400µM EDTA. Pellets were then frozen at -80C until lysis in Triton lysis buffer (1% Triton X-100, 150 mM NaCl, 1 mM Na3VO4, protease inhibitors (Thermo Fisher Scientific), 10 mM Tris pH 7.6) on ice for 45 min. Lysates were centrifuged at 17,000 x *g* at 4℃ for 10 min, and the liquid phase was collected for usage in downstream applications. When necessary, the total protein content of the lysates was quantified (BCA Assay Kit, Thermo Fisher Scientific) and equalized among samples. Images were captured with a *Chemidoc* luminescence acquiring system (BioRad) and analyzed digitally (Image Lab, BioRad). The densities of phospho-proteins were normalized by their total counterparts, and the density of total proteins was normalized to the loading control. For total protein loading control, we used TGX Stain-Free™ FastCast™ Acrylamide Kits, 7.5 or 10%(Biorad, 1610183) or added 0.5% v/v Tri-Chloro-ethanol (TCE) to acrylamide gel preparations (*88*). Antibodies used can be found in supplementary methods.

Quantitative real-time polymerase chain analyses

The mRNA expression in isolated murine $CD4^+$ T cells was detected using qRT-PCR. Total RNA was extracted using the RNeasy kit (Qiagen), quantified using a NanoDrop ND- (Thermo Fisher Scientific), and transcribed into cDNA with the Superscript III™ Reverse Transcriptase (Thermo Fisher Scientific). Quantitative real-time PCR was performed with FastStart essential DNA green master (Roche, Diagnostics) using Bio-Rad CFX96 Real-Time System. CFX Maestro software was used for the analysis of the qPCR data (Bio-Rad). Primer sequences: Taok3: 5'-TCCGCGTCTTTGGTTACACGGC-3' and 5'-GCGCCGCATCCGCTTATAACCT-3'; Shp-1: 5' - TTTGCGACGCTGACAGAGCTGG -3' and 5' - GGCCGTGGTACCACCTCTCACT -3'; Hprt1: 5'-AAGCTTGCTGGTGAAAAGA-3' and 5'-CAAGGGCATATCCAACAACA-3'; Hmbs: 5'-AGGTCCCTGTTCAGCAAGAA-3' and 5'-CTTGGAATGTTACGGGCAGT-3.

Immunoprecipitations and kinase reaction

For all the transfections performed in HEK293 T cells, Lipofectamine 2000 (Thermo Fisher Scientific, 11668019) reagent was used. In most assays, 500µg of protein was used for IP. Briefly, cells were lysed in IP buffer (20mM Tris pH7.4, 100mM NaCl 1% Triton and a complete protease inhibitor cocktail). The lysates were centrifuged for 10min, 13,000rpm to get rid of cell debris/DNA and pre-cleared with a 10% slurry of agarose beads for 30 minutes (A-1040S-500, Agarose Bead technologies). IP with anti-FLAG M2 agarose beads was 2 hours, 4°C, and beads were washed 5 times with IP buffer prior to resuspension in 1X Laemmli buffer. Samples were boiled before loading on gel. For endogenous TAOK3-IP in Jurkat T cells, 1500µg was used. There, cells were lysed and pre-cleared as described above, and 1500µg of lysate was incubated

overnight, at 4°C, with 4uL Dynabeads (10001D, Termofisher scientific) A and 2uL Taok3 antibody (Proteintech 10158-2-AP, Proteintech) per reaction. For the detection of a substrate trapping phenotype on TAOK3, we mutated C453S and D419A in the SHP-1-pDEST26-c-FLAG. The C453S mutation of SHP-1 allows binding of the physiological substrate and leads to the stabilization of the enzyme-substrate interaction. On the other hand replacing the aspartate maintains the WDP-loop over the phospho-tyrosine substrate and thus prevents the substrate from undocking. In these mutants, a putative substrate would have increased co-immunoprecipitation upon SHP-1 IP (*89, 90*). Kinase reaction for detection of phosphorylated residues on SHP-1. For the detection of phosphorylated SHP-1 residues, we first incubated FLAG-SHP-1 (aa1-595) with or without GST-TAOK3 (aa1.-411) (Sino biological, 11547-H20B) in Kinase buffer (50mM Tris pH7.5, 20mM MgCL2, 2mM DTT) in the presence of 1uM ATP. Briefly, TAOK3 and substrate were incubated at room temperature in Kinase buffer for 30 minutes in a ratio of 1:4 (for SHP-1). Reactions were then kept at -80C until analysis by mass spectrometry. For

Flow-cytometry

Staining and washing were performed in round bottom polystyrene 5mL tubes (Falcon, 14-959-6). Unless otherwise stated, intracellular staining was performed with the Foxp3/Transcription Factor Fixation/Permeabilization solution. (eBioscience) according to the manufacturer's protocol. For calcium incorporation assays, cells were incubated for 45 minutes at 37C with loading media (RPMI 1640, 2% FBS, 20 mM HEPES and 50 µM ß-mercaptoethanol containing 4µg/mL Fluo-4AM (InVitrogen, F14201), 2.5 mM

probenecid (Sigma-Aldrich, P8761-25G) and 0.02% Pluronic® F-127 (Sigma-Aldrich, P2443-250G). Cells were washed once with PBS before de-esterification with HBSS supplemented with 20 mM HEPES, 1mM $CaCl_2$, 1mM $MgSO_4$ and 50 µM ß-mercaptoethanol for 30 minutes at room temperature. Cells were subsequently washed with PBS before incubation with biotin-conjugated anti-CD3 antibody for 30 minutes on ICE. 1µg/mL Ionomycin (Sigma-Aldrich, 407953) was used as a positive control for calcium incorporation. Intracellular staining for phospho-Lck-Tyr^{505} was realized with True-Phos™ Perm Buffer (Biolegend) and according to the manufacturer's protocol. Secondary antibody Anti-rabbit secondary antibody conjugated to Alexa Fluor 488 was used for detection (1:500 dilution). The data acquisition was made with the 5-laser LSR FORTRESSA from BD operated with the BD DIVA software. Data were analyzed using FlowJo. V10 software. Antibodies and dilution used can be found in supplementary methods.

Antibodies

Antibodies for immunoblotting: The antibodies with the indicated dilutions were as follows: anti-pS536 (p65-NF-κB) (Cell signaling Technologies, 3033S, 1:1000), anti- NF-κB (Cell signaling Technologies, 8242S, 1:2000), monoclonal anti-TAOK3 (Abcam, ab150388, 1:1000), anti-pT183/Y185 (JNK) (Cell signaling Technologies, 9251S, 1:1000), anti-JNK (Cell signaling Technologies, 9252S, 1:2000), anti-pT180/Y182 (p38) (Cell signaling Technologies, 4511S, 1:1000), anti-p38 (Cell signaling Technologies, 8690S, 1:2000), anti-V5 tag (InvivoGen, 46-0705, 1:1000), anti-actin (Sigma, A4700, 1:6000), anti-pT202/Y204 (ERK) (Cell signaling Technologies, 4377S, 1:1000), anti-

ERK (Cell signaling Technologies, 4695S, 1:2000), polyclonal anti-TAOK3 (Abcam, 70297, 1:1000), anti-pTyr^{394} (Lck) (R&D, MAB7500, 1:1000), anti-pTyr^{394} (Lck) (Cell signaling technologies, 70926S, 1:1000), anti-Lck (Cell signaling Technologies, 2752S, 1:2000), monoclonal anti-TAOK3 (Abcam, ab150388, 1:1000), anti-vinculin (Sigma, V9131, 1:3000), anti-SHP-1 (Cell signaling Technologies, 3759S, 1:2000), anti-Tyr^{505} (Lck) (Cell signaling Technologies, 2751S, 1:1000), anti-CAS9 (Abcam, 189380, 1:1000), anti-FLAG tag (Cell signaling Technologies, 14793S, 1:3000), anti-SRC (Cell signaling Technologies, 2110S, 1:2000), anti-GAPDH (Sigma, MAB374, 1:6000), anti-pY536 (SHP-1) (Abcam, 41437, 1:1000), anti-HA tag (Cell signaling Technologies, 3724S, 1:3000).

Antibodies for Flow cytometry: APC anti-IL-2 (BD Pharmigen, 562041, 1:50), BV421 anti-CD44 Clone (BD Pharmigen, 563970, 1:600), BV786 Anti-CD62L (BD Pharmigen, 564109, 1:400) and PerCP-Cy5.5 anti-CD122 (BD Pharmigen, 564764, 1:200), Alexa-Fluor 488 Anti-IgG (Biolegend, minimal x-reactivity, 1:500) Donkey Polyclonal Antibody (Biolegend, 406416, 1:500), APC/Cy7 anti-CD4 (Biolegend, 100413, 1:400), PE anti-CD4 (Biolegend, 100407, 1:500), APC Anti-CD3ε (Biolegend, 100311, 1:200), FITC Anti-CD3ε (Biolegend, 100306, 1:200), PE/Cy5 anti-mouse CD8a (Biolegend, 553034, 1:400), APC anti-CCR4 (Biolegend, 131211, 1:100), Biotin anti-CXCR3 (Biolegend, 126503 ,1:400), PE anti-T-bet (Biolegend, 644809, 1:100), APC anti-PD-1 (Biolegend, 135209 , 1:200), BV786 anti-IL7Rα (Biolegend, 135037, 1:200), PerCp cy5.5 anti-CD69 (Biolegend, 104521, 1:300), PE Anti-CD25 (Biolegend, 101904, 1:300), PeCy7 anti-CD25 (Biolegend, 101915 , 1:300), PerCp anti-CD28 (Thermo-fisher, MA1-10171, 1:100), PeCy7 anti-CD44 (Thermo-fisher, 25-0441-81, 1:700)BV650-Streptavidin

(Biolegend, 405231, 1:2000). Stains: LIVE/DEAD™ Fixable Blue Dead Cell Stain Kit for UV excitation (Thermo-fisher, L34961, 1:1000), CellTrace™ CFSE Cell Proliferation Kit, for flow cytometry (Thermo-fisher, C34554, 1:1000).

Viral transduction

For the stable expression cell lines, the transfer plasmids consisted of the pLenti6-Taok3-V5 and the mutant versions (T181A Y183F, Y256F, Y305F, and S324A). Transduction was conducted via lipofection. The packaging and envelope plasmids were psPAX2 (12260) and pMD2.G (12259), respectively, and were purchased from Addgene. For lentiviral vectors, the *Taok3* complete ORF was in pLenti6/V5 DEST (Thermo Fisher Scientific, V49610). Site-directed mutagenesis was performed as described in (*91*) to generate mutants T181AY183F-V5, Y256F-V5, Y305F-V5, and S324A-V5. Briefly, pLenti6-*Taok3* was used as a PCR template for amplification with a high-fidelity polymerase (Kapa HiFi, Roche) primer containing point mutations. All constructs were sequenced to confirm the correct insertion of the amplicon and the presence of the desired mutations. Production of lentiviral particles and transduction was described in (*26*).

Plasmids

The SHP-1 (PTPN6) complete ORF was inserted in pDEST26-c-FLAG. All subsequent mutations and truncated mutants were cloned from that vector. SHP-1 WT (amino acid 1-595), SHP-1ΔC72 (aa 1-523), SHP-1ΔNSH2 (aa 110-595), SHP-1ΔNSH2-CSH2 (aa 243-595), SHP-1N-SH2, C-SH2 (aa 1-213), SHP-1 C-term (aa 523-595). The *Taok3*

entire ORF was inserted in the pcDNA 3.1 backbone. For the TET-ON TAOK3-V5 Jurkat cell line, we inserted the *Taok3* complete ORF in pLenti-puro (Addgene, 39481) before sub-cloning it, along with the CMV promoter and Tet operators, into pLenti6/V5 DEST (Thermo Fisher Scientific, V49610). HA-tagged Ubiquitin vector was purchased from Addgene (Addgene, 18712).

TCR stimulation

Ex vivo T cells were stimulated with plate-bound CD3 (2µg/mL, 10µg/mL, or a concentration range) and soluble CD28 (5µg/mL). Prior to stimulation, the functional grade CD3 antibody (Thermo Fischer Scientific, 16-0031-86) was diluted in PBS. For functional assays: (24-72h) incubated in tissue-culture-treated 96 well plates overnight (16h) at 4℃. Plates were then washed once with sterile PBS before the addition of the T cell suspensions. 20U/mL of recombinant murine IL-2 (Preprotech, 212-12) was supplemented when culturing Naïve CD4 T cells assays. IL-2 was not supplemented when 24h ELISA cytokine quantification was realized (Fig. 2). The functional grade anti-CD28 (Thermo Fischer Scientific, 16-0281-86) was used in suspension at 5µg/mL unless stated otherwise. For signaling: (0-30minutes) Short-term stimulations of Jurkat cells (1x106) and Jurkat Taok3 mutants (KO, V5-WT, Y181F Y183F, Y256F, Y305F, and S324A) were done using soluble 10µg/mL anti-CD3 (Life Technologies, 16-0038-85, clone UCHT1), 5µg/mL anti-CD28 (Life Technologies, 16-0289-85, clone CD28.2) and 10µg/mL F(ab')2-Goat anti-Mouse IgG serving as a cross-linker (Life Technologies, 16-5098-85). For $CD4^+$ isolated mouse splenocytes, similar short-term stimulation was realized with anti-mouse antibodies already described in the reagents section and with

anti-Armenian hamster rabbit IgG serving as a cross-linker (Thomas scientific, 307-005-003). For pharmacological inhibition of Shp-1/2, we used 0 to 4μM of NSC-87877 (Selleck Chemicals, S8182) at the same time as plate bound CD3 (5μg/mL) and soluble CD28 stimulation (5μg/mL). Cells were maintained in stimulation without the addition of exogenous IL-2 for a total of 48-hours. These isolated $CD4^+$ T naïve T cells were not pre-treated with the inhibitor prior to the stimulation/expansion.

Live-cell imaging

Tissue culture plates were treated with poly-L-lysine according to the manufacturer's protocol (Sigma, P4707). Jurkat-derived cell lines were plated in 96 well plates (5×10^3 cells per well) and cultured in an IncuCyte cell culture system (Essen Bioscience). Images of live cells were captured every 4 hours for 7 days (4 images per well, 200x magnification) to track the growth of mutants at steady state. Growth curves were digitally generated, and the confluence slope at the linear phase was calculated to determine the rate of growth (%confluence/hour).

Enzyme-linked immunosorbent assays (ELISAs) and multiplexing

Doxycycline-treated mouse T cells (5×10^4 in 1 ml of medium) were cultured in 24-well plates and stimulated with plate-bound anti-CD3 (2 μg/ml) and soluble anti-CD28 (5 μg/ml). Supernatants were collected after 1 and 4 days of stimulation. Accumulation of IL-2 in the supernatants was quantified by ELISA according to the manufacturer's protocol (BMS601, Thermo Fisher Scientific). Supernatants of primary $CD4^+$ T cells stimulated with rangof of concentrations of plate-bound anti-CD3 and soluble anti-CD28

(5µg/mL) were collected 24h after, and IL-2 was quantified using ELISA MAX™ Deluxe Set Mouse IL-2 (431004, Biolegend). For cytokine multiplexing, serum or supernatants were diluted one fold in PBS before being sent to EVE Technologies, Calgary, Alberta, Canada, for cytokine multiplexing with a Bio-Plex 200.

CFSE staining for quantitative proliferation analysis

Naïve $CD4^+$ T cells were stained with CFSE according to the manufacturer's protocol (C34554, Life Technologies, 1:1000). After 72h of culture with stimulants, cells were harvested and analyzed with the 5-laser LSR Fortessa from BD. The average distribution of daughter generation was calculated from the technical and biological replicates of each condition.

Protein purification

HEK-293 cells were transfected using 15ug FLAG-SHP-1 (aa1-595) plasmid: 30uL Lipofectamine 2000 OptiMem media per 15cm plate. Confluent plates were lysed in Lysis buffer: 20mM Tris pH 7.4, 300mM NaCl, 1% Triton and complete protease inhibitor. DNA/cell debris were removed by centrifugation at 13,000rpm for 10 minutes, 4°C. The lysate was incubated with FLAG-Agarose M2 beads for 2 hours before transferring the agarose beads to an empty PD-10 column. Beads were washed 4X using 10CV lysis buffer followed by one wash with TBS pH7.5. The protein was eluted 6*2CV using 100ug/mL FLAG peptide in TBS. Eluted proteins were concentrated on AMICON Ultra-4. Cut-off 30K glycerol was added for a final concentration of 15-20%

along with 1mM DTT. Protein purity was evaluated by gel migration and Coomassie blue staining.

Affinity purification mass spectrometry

HEK293T/17 cells were transfected with SHP-1 (FLAG) and co-transfected with or without TAOK3 and/or SRC_{Y527F}. Cell lysates were subjected to M2-FLAG immunoprecipitation as per the previously described method. Co-IP sample beads were loaded onto a single stacking gel band to remove lipids, detergents, and salts. The single gel band containing all proteins was reduced with DTT, alkylated with iodoacetic acid, and digested with trypsin. 2 µg of extracted peptides were re-solubilized in 0.1% aqueous formic acid and loaded onto a Thermo Acclaim Pepmap (Thermo, 75uM ID X 2cm C18 3uM beads) pre-column and then onto an Acclaim Pepmap Easyspray (Thermo, 75uM X 15cm with 2uM C18 beads) analytical column separation using a Dionex Ultimate 3000 uHPLC at 250 nL/min with a gradient of 2-35% organic (0.1% formic acid in acetonitrile) over 2 hours. Peptides were analyzed using a Thermo Orbitrap Fusion mass spectrometer operating at 120,000 resolution (FWHM in MS1) with HCD sequencing (15,000 resolution) at top speed for all peptides with a charge of 2+ or greater. The raw data were converted into *.mgf format (Mascot generic format) for searching using the Mascot 2.6.2 search engine (Matrix Science) against Human Uniprot sequences (2022). The database search results were loaded onto Scaffold Q+ Scaffold_4.9.0 (Proteome Sciences) for statistical treatment and initial data visualization. Further analysis was realized with the Prohitz visualization tool (*92*).

Protein interaction networks and molecular function were visualized using the GeneMania online tool (*40*).

Statistical analysis and data visualization

Protein interaction modeling was conducted in Pymol upon initial docking with HADDOCK2.4 (*93, 94*) using the rigid AlphaFold structures for SHP-1 (P29350) and TAOK3 (Q9H2K8) (*95, 96*). Statistical analysis was done using Graphpad prism V9.0. Briefly, ratio paired t-tests were performed upon validation of Gaussian distribution with the Anderson-Darling normality test. If normality was not reached, equivalent non-parametric tests were used to compare the difference in means between the two groups. For more than two groups, one and two-way ANOVA with matching biological replicates and Dunnett's multiple comparison test were used. To objectively measure the significance in proliferation distributions from Fig. 2, χ^2 tests were realized by comparing the percentages distribution of each daughter generation from the average of technical and biological from each genotype (Generation 0& G1, G2, G3, G4, G5, and G6+). G0 and G1 generations had to be pooled to meet the χ^2 statistical test criteria ($n_{/group} \geq 5$). Significance was considered at p-values < 0.05.

Supplementary Materials

Figs. S1–S6.

References and Notes

1. X. Su, J. A. Ditlev, E. Hui, W. Xing, S. Banjade, J. Okrut, D. S. King, J. Taunton, M. K. Rosen, R. D. Vale, Phase separation of signaling molecules promotes T cell receptor signal transduction. *Science* **352**, 595 (2016)10.1126/science.aad9964).

2. B. A. Irving, A. Weiss, The cytoplasmic domain of the T cell receptor zeta chain is sufficient to couple to receptor-associated signal transduction pathways. *Cell* **64**, 891-901 (1991); published online EpubMar 8 (10.1016/0092-8674(91)90314-o).
3. R. J. Salmond, A. Filby, I. Qureshi, S. Caserta, R. Zamoyska, T-cell receptor proximal signaling via the Src-family kinases, Lck and Fyn, influences T-cell activation, differentiation, and tolerance. *Immunological Reviews* **228**, 9-22 (2009)10.1111/j.1600-065x.2008.00745.x).
4. U. Lorenz, SHP-1 and SHP-2 in T cells: two phosphatases functioning at many levels. *Immunological Reviews* **228**, 342-359 (2009)10.1111/j.1600-065x.2008.00760.x).
5. A. K. Chakraborty, A. Weiss, Insights into the initiation of TCR signaling. *Nat Immunol* **15**, 798-807 (2014); published online EpubSep (10.1038/ni.2940).
6. J. Shaw, P. Utz, D. Durand, J. Toole, E. Emmel, G. Crabtree, Identification of a putative regulator of early T cell activation genes. *Science* **241**, 202-205 (1988)10.1126/science.3260404).
7. F. Macian, NFAT proteins: key regulators of T-cell development and function. *Nature Reviews Immunology* **5**, 472-484 (2005)10.1038/nri1632).
8. S. H. Ross, D. A. Cantrell, Signaling and Function of Interleukin-2 in T Lymphocytes. *Annual Review of Immunology* **36**, 411-433 (2018)10.1146/annurev-immunol-042617-053352).
9. W. Liao, J.-X. Lin, Warren, Interleukin-2 at the Crossroads of Effector Responses, Tolerance, and Immunotherapy. *Immunity* **38**, 13-25 (2013)10.1016/j.immuni.2013.01.004).
10. T. R. Malek, I. Castro, Interleukin-2 Receptor Signaling: At the Interface between Tolerance and Immunity. *Immunity* **33**, 153-165 (2010)10.1016/j.immuni.2010.08.004).
11. Z. Taha, H. J. Janse van Rensburg, X. Yang, The Hippo Pathway: Immunity and Cancer. *Cancers (Basel)* **10**, (2018); published online EpubMar 28 (10.3390/cancers10040094).
12. D. Zhou, B. D. Medoff, L. Chen, L. Li, X.-f. Zhang, M. Praskova, M. Liu, A. Landry, R. S. Blumberg, V. A. Boussiotis, R. Xavier, J. Avruch, The Nore1B/Mst1 complex restrains antigen receptor-induced proliferation of naïve T cells. *Proceedings of the National Academy of Sciences* **105**, 20321-20326 (2008)doi:10.1073/pnas.0810773105).
13. Y. Ueda, K. Katagiri, T. Tomiyama, K. Yasuda, K. Habiro, T. Katakai, S. Ikehara, M. Matsumoto, T. Kinashi, Mst1 regulates integrin-dependent thymocyte trafficking and antigen recognition in the thymus. *Nat Commun* **3**, 1098 (2012)10.1038/ncomms2105).
14. T. Tomiyama, Y. Ueda, T. Katakai, N. Kondo, K. Okazaki, T. Kinashi, Antigen-specific suppression and immunological synapse formation by regulatory T cells require the Mst1 kinase. *PLoS One* **8**, e73874 (2013)10.1371/journal.pone.0073874).
15. J. E. Thaventhiran, A. Hoffmann, L. Magiera, M. de la Roche, H. Lingel, M. Brunner-Weinzierl, D. T. Fearon, Activation of the Hippo pathway by CTLA-4 regulates the expression of Blimp-1 in the CD8+ T cell. *Proc Natl Acad Sci U S A* **109**, E2223-2229 (2012); published online EpubAug 14 (10.1073/pnas.1209115109).
16. Z. Meng, T. Moroishi, V. Mottier-Pavie, S. W. Plouffe, C. G. Hansen, A. W. Hong, H. W. Park, J. S. Mo, W. Lu, S. Lu, F. Flores, F. X. Yu, G. Halder, K. L. Guan, MAP4K family kinases act in parallel to MST1/2 to activate LATS1/2 in the Hippo pathway. *Nat Commun* **6**, 8357 (2015); published online EpubOct 5 (10.1038/ncomms9357).
17. C. L. Poon, J. I. Lin, X. Zhang, K. F. Harvey, The sterile 20-like kinase Tao-1 controls tissue growth by regulating the Salvador-Warts-Hippo pathway. *Dev Cell* **21**, 896-906 (2011); published online EpubNov 15 (10.1016/j.devcel.2011.09.012).
18. S. W. Plouffe, Z. Meng, K. C. Lin, B. Lin, A. W. Hong, J. V. Chun, K. L. Guan, Characterization of Hippo Pathway Components by Gene Inactivation. *Mol Cell* **64**, 993-1008 (2016); published online EpubDec 1 (10.1016/j.molcel.2016.10.034).
19. C.-Y. Fang, T.-C. Lai, M. Hsiao, Y.-C. Chang, The Diverse Roles of TAO Kinases in Health and Diseases. *International Journal of Molecular Sciences* **21**, 7463 (2020)10.3390/ijms21207463).

20. Z. Chen, M. Raman, L. Chen, S. F. Lee, A. G. Gilman, M. H. Cobb, TAO (Thousand-and-one Amino Acid) Protein Kinases Mediate Signaling from Carbachol to p38 Mitogen-activated Protein Kinase and Ternary Complex Factors. *Journal of Biological Chemistry* **278**, 22278-22283 (2003)10.1074/jbc.m301173200).
21. J. T. Yustein, L. Xia, J. M. Kahlenburg, D. Robinson, D. Templeton, H.-J. Kung, Comparative studies of a new subfamily of human Ste20-like kinases: homodimerization, subcellular localization, and selective activation of MKK3 and p38. *Oncogene* **22**, 6129-6141 (2003)10.1038/sj.onc.1206605).
22. H. Hammad, M. Vanderkerken, P. Pouliot, K. Deswarte, W. Toussaint, K. Vergote, L. Vandersarren, S. Janssens, I. Ramou, S. N. Savvides, J. J. Haigh, R. Hendriks, M. Kopf, K. Craessaerts, B. de Strooper, J. F. Kearney, D. H. Conrad, B. N. Lambrecht, Transitional B cells commit to marginal zone B cell fate by Taok3-mediated surface expression of ADAM10. *Nat Immunol* **18**, 313-320 (2017); published online EpubMar (10.1038/ni.3657).
23. M. Vanderkerken, B. Maes, L. Vandersarren, W. Toussaint, K. Deswarte, M. Vanheerswynghels, P. Pouliot, L. Martens, S. Van Gassen, C. M. Arthur, M. E. Kirkling, B. Reizis, D. Conrad, S. Stowell, H. Hammad, B. N. Lambrecht, TAO-kinase 3 governs the terminal differentiation of NOTCH2-dependent splenic conventional dendritic cells. *Proceedings of the National Academy of Sciences* **117**, 31331-31342 (2020)10.1073/pnas.2009847117).
24. B. Maes, U. Smole, M. Vanderkerken, K. Deswarte, J. Van Moorleghem, K. Vergote, M. Vanheerswynghels, C. De Wolf, S. De Prijck, N. Debeuf, B. Pavie, W. Toussaint, S. Janssens, S. Savvides, B. N. Lambrecht, H. Hammad, The STE20 kinase TAOK3 controls the development house dust mite–induced asthma in mice. *Journal of Allergy and Clinical Immunology*, (2021); published online Epub2021/09/08/ (https://doi.org/10.1016/j.jaci.2021.08.020).
25. A. Poirier, C. Wu, A. M. Hincapie, Z. Martinez-Cordova, B. M. Abidin, M. L. Tremblay, TAOK3 limits age-associated inflammation by negatively modulating macrophage differentiation and their production of TNFα. *Immunity & Ageing* **20**, 31 (2023); published online Epub2023/07/03 (10.1186/s12979-023-00350-y).
26. J. V. S. Ormonde, Z. Li, C. Stegen, J. Madrenas, TAOK3 Regulates Canonical TCR Signaling by Preventing Early SHP-1–Mediated Inactivation of LCK. *The Journal of Immunology* **201**, 3431-3442 (2018)10.4049/jimmunol.1800284).
27. M. Raman, S. Earnest, K. Zhang, Y. Zhao, M. H. Cobb, TAO kinases mediate activation of p38 in response to DNA damage. *Embo j* **26**, 2005-2014 (2007); published online EpubApr 18 (10.1038/sj.emboj.7601668).
28. P. V. Hornbeck, B. Zhang, B. Murray, J. M. Kornhauser, V. Latham, E. Skrzypek, PhosphoSitePlus, 2014: mutations, PTMs and recalibrations. *Nucleic Acids Res* **43**, D512-520 (2015); published online EpubJan (10.1093/nar/gku1267).
29. M. Cargnello, P. P. Roux, Activation and function of the MAPKs and their substrates, the MAPK-activated protein kinases. *Microbiol Mol Biol Rev* **75**, 50-83 (2011); published online EpubMar (10.1128/mmbr.00031-10).
30. C. Y. Koo, C. Giacomini, M. Reyes-Corral, Y. Olmos, I. A. Tavares, C. M. Marson, S. Linardopoulos, A. N. Tutt, J. D. H. Morris, Targeting TAO Kinases Using a New Inhibitor Compound Delays Mitosis and Induces Mitotic Cell Death in Centrosome Amplified Breast Cancer Cells. *Mol Cancer Ther* **16**, 2410-2421 (2017); published online EpubNov (10.1158/1535-7163.Mct-17-0077).
31. L. Philipsen, A. V. Reddycherla, R. Hartig, J. Gumz, M. Kästle, A. Kritikos, M. P. Poltorak, Y. Prokazov, E. Turbin, A. Weber, W. Zuschratter, B. Schraven, L. Simeoni, A. J. Müller, De novo phosphorylation and conformational opening of the tyrosine kinase Lck act in concert to initiate T cell receptor signaling. *Science Signaling* **10**, eaaf4736 (2017)10.1126/scisignal.aaf4736).
32. B. L. Williams, B. J. Irvin, S. L. Sutor, C. C. Chini, E. Yacyshyn, J. Bubeck Wardenburg, M. Dalton, A. C. Chan, R. T. Abraham, Phosphorylation of Tyr319 in ZAP-70 is required for T-cell antigen

receptor-dependent phospholipase C-gamma1 and Ras activation. *Embo j* **18**, 1832-1844 (1999); published online EpubApr 1 (10.1093/emboj/18.7.1832).
33. G. G. Chiang, B. M. Sefton, Specific Dephosphorylation of the Lck Tyrosine Protein Kinase at Tyr-394 by the SHP-1 Protein-tyrosine Phosphatase. *Journal of Biological Chemistry* **276**, 23173-23178 (2001)10.1074/jbc.m101219200).
34. M. Bergman, T. Mustelin, C. Oetken, J. Partanen, N. A. Flint, K. E. Amrein, M. Autero, P. Burn, K. Alitalo, The human p50csk tyrosine kinase phosphorylates p56lck at Tyr-505 and down regulates its catalytic activity. *The EMBO Journal* **11**, 2919-2924 (1992)10.1002/j.1460-2075.1992.tb05361.x).
35. L. Chen, S. S. Sung, M. L. Yip, H. R. Lawrence, Y. Ren, W. C. Guida, S. M. Sebti, N. J. Lawrence, J. Wu, Discovery of a novel shp2 protein tyrosine phosphatase inhibitor. *Mol Pharmacol* **70**, 562-570 (2006); published online EpubAug (10.1124/mol.106.025536).
36. S. M. Thomas, J. S. Brugge, CELLULAR FUNCTIONS REGULATED BY SRC FAMILY KINASES. *Annual Review of Cell and Developmental Biology* **13**, 513-609 (1997)10.1146/annurev.cellbio.13.1.513).
37. A.-K. Somani, J. S. Bignon, G. B. Mills, K. A. Siminovitch, D. R. Branch, Src Kinase Activity Is Regulated by the SHP-1 Protein-tyrosine Phosphatase *. *Journal of Biological Chemistry* **272**, 21113-21119 (1997)10.1074/jbc.272.34.21113).
38. C. Blanchetot, M. Chagnon, N. Dube, M. Halle, M. Tremblay, Substrate-trapping techniques in the identification of cellular PTP targets. *Methods* **35**, 44-53 (2005)10.1016/j.ymeth.2004.07.007).
39. F. Mercan, A. M. Bennett, Analysis of protein tyrosine phosphatases and substrates. *Current protocols in molecular biology* **Chapter 18**, Unit-18.16 (2010)10.1002/0471142727.mb1816s91).
40. M. Franz, H. Rodriguez, C. Lopes, K. Zuberi, J. Montojo, G. D. Bader, Q. Morris, GeneMANIA update 2018. *Nucleic Acids Res* **46**, W60-w64 (2018); published online EpubJul 2 (10.1093/nar/gky311).
41. D. H. Lee, A. L. Goldberg, Proteasome inhibitors: valuable new tools for cell biologists. *Trends Cell Biol* **8**, 397-403 (1998); published online EpubOct (10.1016/s0962-8924(98)01346-4).
42. J. M. Chemnitz, R. V. Parry, K. E. Nichols, C. H. June, J. L. Riley, SHP-1 and SHP-2 Associate with Immunoreceptor Tyrosine-Based Switch Motif of Programmed Death 1 upon Primary Human T Cell Stimulation, but Only Receptor Ligation Prevents T Cell Activation. *The Journal of Immunology* **173**, 945-954 (2004)10.4049/jimmunol.173.2.945).
43. Q. Xiao, X. Li, Y. Li, Z. Wu, C. Xu, Z. Chen, W. He, Biological drug and drug delivery-mediated immunotherapy. *Acta Pharmaceutica Sinica B* **11**, 941-960 (2021); published online Epub2021/04/01/ (https://doi.org/10.1016/j.apsb.2020.12.018).
44. Q. Liang, D. Ma, X. Zhu, Z. Wang, T. T. Sun, C. Shen, T. Yan, X. Tian, T. Yu, F. Guo, J. Tang, Y. Lin, H. Chen, C. Zhou, Z. Ge, M. Zhong, J. Chen, Q. Liu, Z. Wang, J. Y. Fang, H. Chen, J. Hong, RING-Finger Protein 6 Amplification Activates JAK/STAT3 Pathway by Modifying SHP-1 Ubiquitylation and Associates with Poor Outcome in Colorectal Cancer. *Clin Cancer Res* **24**, 1473-1485 (2018); published online EpubMar 15 (10.1158/1078-0432.Ccr-17-2133).
45. J. Zhang, H. Wu, B. Yi, J. Zhou, L. Wei, Y. Chen, L. Zhang, RING finger protein 38 induces gastric cancer cell growth by decreasing the stability of the protein tyrosine phosphatase SHP-1. *FEBS Lett* **592**, 3092-3100 (2018); published online EpubSep (10.1002/1873-3468.13225).
46. Y. Bian, L. Yuan, X. Yang, L. Weng, Y. Zhang, H. Bai, J. Chen, SMURF1-mediated ubiquitylation of SHP-1 promotes cell proliferation and invasion of endometrial stromal cells in endometriosis. *Ann Transl Med* **9**, 362 (2021); published online EpubMar (10.21037/atm-20-2897).
47. D. Aki, H. Li, W. Zhang, M. Zheng, C. Elly, J. H. Lee, W. Zou, Y.-C. Liu, The E3 ligases Itch and WWP2 cooperate to limit TH2 differentiation by enhancing signaling through the TCR. *Nature*

Immunology **19**, 766-775 (2018); published online Epub2018/07/01 (10.1038/s41590-018-0137-8).

48. J.-F. Cloutier, A. Veillette, Cooperative Inhibition of T-Cell Antigen Receptor Signaling by a Complex between a Kinase and a Phosphatase. *Journal of Experimental Medicine* **189**, 111-121 (1999)10.1084/jem.189.1.111).
49. A. Gjörloff-Wingren, M. Saxena, S. Williams, D. Hammi, T. Mustelin, Characterization of TCR-induced receptor-proximal signaling events negatively regulated by the protein tyrosine phosphatase PEP. *Eur J Immunol* **29**, 3845-3854 (1999); published online EpubDec (10.1002/(sici)1521-4141(199912)29:12<3845::Aid-immu3845>3.0.Co;2-u).
50. F. Wiede, B. J. Shields, S. H. Chew, K. Kyparissoudis, C. van Vliet, S. Galic, M. L. Tremblay, S. M. Russell, D. I. Godfrey, T. Tiganis, T cell protein tyrosine phosphatase attenuates T cell signaling to maintain tolerance in mice. *J Clin Invest* **121**, 4758-4774 (2011); published online EpubDec (10.1172/jci59492).
51. J. P. Li, C. Y. Yang, H. C. Chuang, J. L. Lan, D. Y. Chen, Y. M. Chen, X. Wang, A. J. Chen, J. W. Belmont, T. H. Tan, The phosphatase JKAP/DUSP22 inhibits T-cell receptor signalling and autoimmunity by inactivating Lck. *Nat Commun* **5**, 3618 (2014); published online EpubApr 9 (10.1038/ncomms4618).
52. C. J. Miller, H. J. Lou, C. Simpson, B. van de Kooij, B. H. Ha, O. S. Fisher, N. L. Pirman, T. J. Boggon, J. Rinehart, M. B. Yaffe, R. Linding, B. E. Turk, Comprehensive profiling of the STE20 kinase family defines features essential for selective substrate targeting and signaling output. *PLOS Biology* **17**, e2006540 (2019)10.1371/journal.pbio.2006540).
53. J. L. Johnson, T. M. Yaron, E. M. Huntsman, A. Kerelsky, J. Song, A. Regev, T.-Y. Lin, K. Liberatore, D. M. Cizin, B. M. Cohen, N. Vasan, Y. Ma, K. Krismer, J. T. Robles, B. van de Kooij, A. E. van Vlimmeren, N. Andrée-Busch, N. F. Käufer, M. V. Dorovkov, A. G. Ryazanov, Y. Takagi, E. R. Kastenhuber, M. D. Goncalves, B. D. Hopkins, O. Elemento, D. J. Taatjes, A. Maucuer, A. Yamashita, A. Degterev, M. Uduman, J. Lu, S. D. Landry, B. Zhang, I. Cossentino, R. Linding, J. Blenis, P. V. Hornbeck, B. E. Turk, M. B. Yaffe, L. C. Cantley, An atlas of substrate specificities for the human serine/threonine kinome. *Nature* **613**, 759-766 (2023); published online Epub2023/01/01 (10.1038/s41586-022-05575-3).
54. A. Markovics, D. M. Toth, T. T. Glant, K. Mikecz, Regulation of autoimmune arthritis by the SHP-1 tyrosine phosphatase. *Arthritis Research & Therapy* **22**, 160 (2020); published online Epub2020/06/26 (10.1186/s13075-020-02250-8).
55. S. Choi, J. Lee, T. Hatzihristidis, G. Gaud, A. Dutta, A. Arya, L. M. Clubb, D. B. Stamos, A. Markovics, K. Mikecz, P. E. Love, THEMIS increases TCR signaling in CD4(+)CD8(+) thymocytes by inhibiting the activity of the tyrosine phosphatase SHP1. *Sci Signal* **16**, eade1274 (2023); published online EpubMay 9 (10.1126/scisignal.ade1274).
56. D. J. Johnson, L. I. Pao, S. Dhanji, K. Murakami, P. S. Ohashi, B. G. Neel, Shp1 regulates T cell homeostasis by limiting IL-4 signals. *Journal of Experimental Medicine* **210**, 1419-1431 (2013)10.1084/jem.20122239).
57. B. J. Pulverer, J. M. Kyriakis, J. Avruch, E. Nikolakaki, J. R. Woodgett, Phosphorylation of c-jun mediated by MAP kinases. *Nature* **353**, 670-674 (1991); published online Epub1991/10/01 (10.1038/353670a0).
58. V. Atsaves, V. Leventaki, G. Z. Rassidakis, F. X. Claret, AP-1 Transcription Factors as Regulators of Immune Responses in Cancer. *Cancers (Basel)* **11**, (2019); published online EpubJul 23 (10.3390/cancers11071037).
59. W. Wen, W. Liu, J. Yan, M. Zhang, Structure basis and unconventional lipid membrane binding properties of the PH-C1 tandem of rho kinases. *J Biol Chem* **283**, 26263-26273 (2008); published online EpubSep 19 (10.1074/jbc.M803417200).

60. K. N. Al-Zahrani, K. D. Baron, L. A. Sabourin, Ste20-like kinase SLK, at the crossroads: a matter of life and death. *Cell Adh Migr* **7**, 1-10 (2013); published online EpubJan-Feb (10.4161/cam.22495).
61. H. Bagci, N. Sriskandarajah, A. Robert, J. Boulais, I. E. Elkholi, V. Tran, Z.-Y. Lin, M.-P. Thibault, N. Dubé, D. Faubert, D. R. Hipfner, A.-C. Gingras, J.-F. Côté, Mapping the proximity interaction network of the Rho-family GTPases reveals signalling pathways and regulatory mechanisms. *Nature Cell Biology* **22**, 120-134 (2020)10.1038/s41556-019-0438-7).
62. M. Faroudi, M. Hons, A. Zachacz, C. Dumont, R. Lyck, J. V. Stein, V. L. J. Tybulewicz, Critical roles for Rac GTPases in T-cell migration to and within lymph nodes. *Blood* **116**, 5536-5547 (2010)10.1182/blood-2010-08-299438).
63. R. El Masri, J. Delon, RHO GTPases: from new partners to complex immune syndromes. *Nature Reviews Immunology* **21**, 499-513 (2021); published online Epub2021/08/01 (10.1038/s41577-021-00500-7).
64. T. H. Ng, G. J. Britton, E. V. Hill, J. Verhagen, B. R. Burton, D. C. Wraith, Regulation of adaptive immunity; the role of interleukin-10. *Front Immunol* **4**, 129 (2013)10.3389/fimmu.2013.00129).
65. K. Adachi, M. M. Davis, T-cell receptor ligation induces distinct signaling pathways in naive vs. antigen-experienced T cells. *Proceedings of the National Academy of Sciences* **108**, 1549-1554 (2011)10.1073/pnas.1017340108).
66. C. Li, P. Beavis, A. C. Palfreeman, P. Amjadi, A. Kennedy, F. M. Brennan, Activation of p38 mitogen-activated protein kinase is critical step for acquisition of effector function in cytokine-activated T cells, but acts as a negative regulator in T cells activated through the T-cell receptor. *Immunology* **132**, 104-110 (2011)10.1111/j.1365-2567.2010.03345.x).
67. C. Dong, D. D. Yang, C. Tournier, A. J. Whitmarsh, J. Xu, R. J. Davis, R. A. Flavell, JNK is required for effector T-cell function but not for T-cell activation. *Nature* **405**, 91-94 (2000); published online EpubMay 4 (10.1038/35011091).
68. Y. Xia, M. Caputo, E. Cansby, S. K. Anand, S. Sütt, M. Henricsson, R. Porosk, H.-U. Marschall, M. Blüher, M. Mahlapuu, STE20-type kinase TAOK3 regulates hepatic lipid partitioning. *Molecular Metabolism* **54**, 101353 (2021); published online Epub2021/12/01/ (https://doi.org/10.1016/j.molmet.2021.101353).
69. E. Tassi, Z. Biesova, P. P. Di Fiore, J. S. Gutkind, W. T. Wong, Human JIK, a novel member of the STE20 kinase family that inhibits JNK and is negatively regulated by epidermal growth factor. *J Biol Chem* **274**, 33287-33295 (1999); published online EpubNov 19 (10.1074/jbc.274.47.33287).
70. Z. Li, H. Oh, M. Cung, S. J. Marquez, J. Sun, H. Hammad, S. Janssens, P. Pouliot, B. N. Lambrecht, Y.-S. Yang, J.-H. Shim, M. B. Greenblatt, TAOK3 is a MAP3K contributing to osteoblast differentiation and skeletal mineralization. *Biochemical and Biophysical Research Communications* **531**, 497-502 (2020); published online Epub2020/10/22/ (https://doi.org/10.1016/j.bbrc.2020.07.060).
71. D. Kapfhamer, I. King, M. E. Zou, J. P. Lim, U. Heberlein, F. W. Wolf, JNK Pathway Activation Is Controlled by Tao/TAOK3 to Modulate Ethanol Sensitivity. *PLOS ONE* **7**, e50594 (2012)10.1371/journal.pone.0050594).
72. Z. Zhang, Z. Tang, X. Ma, K. Sun, L. Fan, J. Fang, J. Pan, X. Wang, H. An, J. Zhou, TAOK1 negatively regulates IL-17-mediated signaling and inflammation. *Cell Mol Immunol* **15**, 794-802 (2018); published online EpubAug (10.1038/cmi.2017.158).
73. H. C. Chuang, X. Wang, T. H. Tan, MAP4K Family Kinases in Immunity and Inflammation. *Adv Immunol* **129**, 277-314 (2016)10.1016/bs.ai.2015.09.006).
74. X. Wang, J. P. Li, L. L. Chiu, J. L. Lan, D. Y. Chen, J. Boomer, T. H. Tan, Attenuation of T cell receptor signaling by serine phosphorylation-mediated lysine 30 ubiquitination of SLP-76

protein. *J Biol Chem* **287**, 34091-34100 (2012); published online EpubOct 5 (10.1074/jbc.M112.371062).
75. J. W. Shui, J. S. Boomer, J. Han, J. Xu, G. A. Dement, G. Zhou, T. H. Tan, Hematopoietic progenitor kinase 1 negatively regulates T cell receptor signaling and T cell-mediated immune responses. *Nat Immunol* **8**, 84-91 (2007); published online EpubJan (10.1038/ni1416).
76. H. C. Chuang, J. L. Lan, D. Y. Chen, C. Y. Yang, Y. M. Chen, J. P. Li, C. Y. Huang, P. E. Liu, X. Wang, T. H. Tan, The kinase GLK controls autoimmunity and NF-κB signaling by activating the kinase PKC-θ in T cells. *Nat Immunol* **12**, 1113-1118 (2011); published online EpubOct 9 (10.1038/ni.2121).
77. J. L. Johnson, T. M. Yaron, E. M. Huntsman, A. Kerelsky, J. Song, A. Regev, T.-Y. Lin, K. Liberatore, D. M. Cizin, B. M. Cohen, N. Vasan, Y. Ma, K. Krismer, J. T. Robles, B. van de Kooij, A. E. van Vlimmeren, N. Andrée-Busch, N. Käufer, M. V. Dorovkov, A. G. Ryazanov, Y. Takagi, E. R. Kastenhuber, M. D. Goncalves, O. Elemento, D. J. Taatjes, A. Maucuer, A. Yamashita, A. Degterev, R. Linding, J. Blenis, P. V. Hornbeck, B. E. Turk, M. B. Yaffe, L. C. Cantley, A global atlas of substrate specificities for the human serine/threonine kinome. *bioRxiv*, 2022.2005.2022.492882 (2022)10.1101/2022.05.22.492882).
78. S. Iizuka, M. Quintavalle, J. C. Navarro, K. P. Gribbin, R. J. Ardecky, M. M. Abelman, C.-T. Ma, E. Sergienko, F.-Y. Zeng, I. Pass, G. V. Thomas, S. K. McWeeney, C. A. Hassig, A. B. Pinkerton, S. A. Courtneidge, Serine-Threonine Kinase TAO3-Mediated Trafficking of Endosomes Containing the Invadopodia Scaffold TKS5α Promotes Cancer Invasion and Tumor Growth. *Cancer Research* **81**, 1472-1485 (2021)10.1158/0008-5472.can-20-2383).
79. V. M. Bii, C. P. Collins, J. D. Hocum, G. D. Trobridge, Replication-incompetent gammaretroviral and lentiviral vector-based insertional mutagenesis screens identify prostate cancer progression genes. *Oncotarget* **9**, 15451-15463 (2018)10.18632/oncotarget.24503).
80. T. L. Romanuik, G. Wang, R. A. Holt, S. J. Jones, M. A. Marra, M. D. Sadar, Identification of novel androgen-responsive genes by sequencing of LongSAGE libraries. *BMC Genomics* **10**, 476 (2009)10.1186/1471-2164-10-476).
81. T.-C. Lai, C.-Y. Fang, Y.-H. Jan, H.-L. Hsieh, Y.-F. Yang, C.-Y. Liu, P. M.-H. Chang, M. Hsiao, Kinase shRNA screening reveals that TAOK3 enhances microtubule-targeted drug resistance of breast cancer cells via the NF-κB signaling pathway. *Cell Communication and Signaling* **18**, 164 (2020); published online Epub2020/10/21 (10.1186/s12964-020-00600-2).
82. Y. Bian, Y. Teper, L. A. Mathews Griner, T. J. Aiken, V. Shukla, R. Guha, P. Shinn, H.-W. Xin, H. Pflicke, A. S. Powers, D. Li, J.-K. Jiang, P. Patel, S. A. Rogers, J. Aubé, M. Ferrer, C. J. Thomas, U. Rudloff, Target Deconvolution of a Multikinase Inhibitor with Antimetastatic Properties Identifies TAOK3 as a Key Contributor to a Cancer Stem Cell–Like Phenotype. *Molecular Cancer Therapeutics* **18**, 2097-2110 (2019)10.1158/1535-7163.mct-18-1011).
83. C.-Y. Koo, C. Giacomini, M. Reyes-Corral, Y. Olmos, I. A. Tavares, C. M. Marson, S. Linardopoulos, A. N. Tutt, J. D. H. Morris, Targeting TAO Kinases Using a New Inhibitor Compound Delays Mitosis and Induces Mitotic Cell Death in Centrosome Amplified Breast Cancer Cells. *Molecular Cancer Therapeutics* **16**, 2410-2421 (2017)10.1158/1535-7163.mct-17-0077).
84. A. E. Yesilkanal, D. Yang, A. Valdespino, P. Tiwari, A. U. Sabino, L. C. Nguyen, J. Lee, X. H. Xie, S. Sun, C. Dann, L. Robinson-Mailman, E. Steinberg, T. Stuhlmiller, C. Frankenberger, E. Goldsmith, G. L. Johnson, A. F. Ramos, M. R. Rosner, Limited inhibition of multiple nodes in a driver network blocks metastasis. *Elife* **10**, (2021); published online EpubMay 11 (10.7554/eLife.59696).
85. W. C. Skarnes, B. Rosen, A. P. West, M. Koutsourakis, W. Bushell, V. Iyer, A. O. Mujica, M. Thomas, J. Harrow, T. Cox, D. Jackson, J. Severin, P. Biggs, J. Fu, M. Nefedov, P. J. de Jong, A. F. Stewart, A. Bradley, A conditional knockout resource for the genome-wide study of mouse gene function. *Nature* **474**, 337-342 (2011); published online EpubJun 15 (10.1038/nature10163).

86. Prem, Lukas, Sang, M. Camiolo, Colin, C. Miething, C. Scuoppo, J. Zuber, Ross, Scott, Kenneth, R. Sordella, Gregory, Scott, A Rapid and Scalable System for Studying Gene Function in Mice Using Conditional RNA Interference. *Cell* **145**, 145-158 (2011)10.1016/j.cell.2011.03.012).
87. D. Grimm, J. Hagmann, D. Koenig, D. Weigel, K. Borgwardt, Accurate indel prediction using paired-end short reads. *BMC Genomics* **14**, 132 (2013)10.1186/1471-2164-14-132).
88. C. L. Ladner, J. Yang, R. J. Turner, R. A. Edwards, Visible fluorescent detection of proteins in polyacrylamide gels without staining. *Anal Biochem* **326**, 13-20 (2004); published online EpubMar 1 (10.1016/j.ab.2003.10.047).
89. J. F. Timms, K. Carlberg, H. Gu, H. Chen, S. Kamatkar, M. J. Nadler, L. R. Rohrschneider, B. G. Neel, Identification of major binding proteins and substrates for the SH2-containing protein tyrosine phosphatase SHP-1 in macrophages. *Mol Cell Biol* **18**, 3838-3850 (1998); published online EpubJul (10.1128/mcb.18.7.3838).
90. A. J. Flint, T. Tiganis, D. Barford, N. K. Tonks, Development of "substrate-trapping" mutants to identify physiological substrates of protein tyrosine phosphatases. *Proc Natl Acad Sci U S A* **94**, 1680-1685 (1997); published online EpubMar 4 (10.1073/pnas.94.5.1680).
91. L. Zheng, U. Baumann, J. L. Reymond, An efficient one-step site-directed and site-saturation mutagenesis protocol. *Nucleic Acids Res* **32**, e115 (2004); published online EpubAug 10 (10.1093/nar/gnh110).
92. J. Knight, H. Choi, G. Gupta, L. Pelletier, B. Raught, A. Nesvizhskii, A.-C. Gingras, ProHits-viz: A suite of web tools for visualizing interaction proteomics data. *Nature Methods* **14**, 645-646 (2017); published online Epub06/29 (10.1038/nmeth.4330).
93. G. C. P. van Zundert, J. P. G. L. M. Rodrigues, M. Trellet, C. Schmitz, P. L. Kastritis, E. Karaca, A. S. J. Melquiond, M. van Dijk, S. J. de Vries, A. M. J. J. Bonvin, The HADDOCK2.2 Web Server: User-Friendly Integrative Modeling of Biomolecular Complexes. *Journal of Molecular Biology* **428**, 720-725 (2016); published online Epub2016/02/22/ (https://doi.org/10.1016/j.jmb.2015.09.014).
94. R. V. Honorato, P. I. Koukos, B. Jiménez-García, A. Tsaregorodtsev, M. Verlato, A. Giachetti, A. Rosato, A. M. J. J. Bonvin, Structural Biology in the Clouds: The WeNMR-EOSC Ecosystem. *Frontiers in Molecular Biosciences* **8**, (2021); published online Epub2021-July-28 (10.3389/fmolb.2021.729513).
95. M. Varadi, S. Anyango, M. Deshpande, S. Nair, C. Natassia, G. Yordanova, D. Yuan, O. Stroe, G. Wood, A. Laydon, A. Žídek, T. Green, K. Tunyasuvunakool, S. Petersen, J. Jumper, E. Clancy, R. Green, A. Vora, M. Lutfi, M. Figurnov, A. Cowie, N. Hobbs, P. Kohli, G. Kleywegt, E. Birney, D. Hassabis, S. Velankar, AlphaFold Protein Structure Database: massively expanding the structural coverage of protein-sequence space with high-accuracy models. *Nucleic Acids Research* **50**, D439-D444 (2021)10.1093/nar/gkab1061).
96. J. Jumper, R. Evans, A. Pritzel, T. Green, M. Figurnov, O. Ronneberger, K. Tunyasuvunakool, R. Bates, A. Žídek, A. Potapenko, A. Bridgland, C. Meyer, S. A. A. Kohl, A. J. Ballard, A. Cowie, B. Romera-Paredes, S. Nikolov, R. Jain, J. Adler, T. Back, S. Petersen, D. Reiman, E. Clancy, M. Zielinski, M. Steinegger, M. Pacholska, T. Berghammer, S. Bodenstein, D. Silver, O. Vinyals, A. W. Senior, K. Kavukcuoglu, P. Kohli, D. Hassabis, Highly accurate protein structure prediction with AlphaFold. *Nature* **596**, 583-589 (2021); published online Epub2021/08/01 (10.1038/s41586-021-03819-2).

Acknowledgments: We thank all members of the Tremblay laboratory and especially S. Hardy and Y. Zolotarov, for their thorough overview of the manuscript. We thank B.-y. Yoon and D.-Y. Lai for their contributions to the iCRISPR model. We also thank J. Poirier for his insightful comments and criticism. We are grateful for the support of R. Francoeur and A. Godille. We thank the Flow-cytometry and CMARC core facilities of the Life Science complex of McGill University. We highlight the work of R. Michaud, A. Laliberté, and C. Gagné for their care of the mice. We also highlight the work of Lorne Taylor and Amy Wong at the proteomics RI-MUHC. For the generation of the full-body Taok3$^{-/-}$ mice, we thank the JAX KOMP2 team and the NIH common fund U42OD011185. **Funding:** A.P. is a Canderel Studentship and FRSQ doctoral scholarship recipient. J.O. is a recipient of the National Council for Scientific and Technological Development award from Brazil – CNPq – Science Without Borders (249656/2013-2). M.L.T. is a Distinguished James McGill Professor and the holder of the J. and J.L. Levesque Chair in Cancer Research. This work was supported by a Canadian Institute of Health Research Foundation grant to M.L.T. (CIHR FDN-159923), the Richard and Edith Strauss Canada Foundation, and the Aclon Foundation. **Author contributions:** Conceptualization: A.P., J.O., and M.L.T. Methodology: A.P., J.O., I.A., B.M.A., C.F., Z.M.C., A.M.H., and C.W. Investigation: A.P., J.O., I.A., B.M.A., and C.F. Visualization: A.P., J.O., I.A., B.M.A., and C.F. Funding acquisition: M.L.T. and J.M. Project administration: M.L.T. Supervision: B.M.A, L.A.P.Q., and M.L.T. Writing of the original draft: A.P. Manuscript review and editing: A.P., J.O., I.A., B.M.A., C.F., Z.M.C., A.M.H., L.A.P.Q., A.C.G., J.M., and M.L.T. **Competing interests:** The authors declare that they have no competing interests. **Data and materials availability:** The mass spectrometry proteomics data have been deposited to the ProteomeXchange Consortium (http://proteomecentral.proteomexchange.org) via the PRIDE

partner repository with the dataset identifier PXD042497. All other data needed to evaluate the conclusions in the paper are present in the paper or the Supplementary Materials.

Figure Legends

Fig. 1. Genetic deletion of Taok3 decreases naïve CD4$^+$ T cell abundance and survival. (A) Phylogenic tree of the STE20 kinases sharing the highest sequence identity with TAOK3. **(B)** Expression analyses using data extracted from the Database of Immune cell Expression (DICE) ranking transcript fold-change between activated and resting CD4$^+$ and CD8$^+$ naïve T cells (Up, increased in expression; Down, decreased in expression). **(C)** Gating strategy used to define CD3$^+$ T cells in flow-cytometric analysis of splenocytes from *Taok3*$^{+/+}$, *Taok3*$^{+/-}$, and *Taok3*$^{-/-}$ mice. SSC-A, side-scatter. Numbers represent the frequency of this population in splenocytes. **(D)** Total numbers of splenic CD3$^+$ T cells in the indicated genotypes. **(E)** Gating strategy used to define splenic CD4$^+$ and CD8$^+$T cells. The numbers represent the frequency of each population in splenocytes. **(F and G)** Total numbers of splenic CD4$^+$ and CD8$^+$ T cells (F) and splenic CD4/CD8 T cell ratio (G) in the indicated genotypes. **(H)** Gating strategy to define naïve (CD62L^{hi}, CD44^{lo}) effector memory (CD62L^{lo}, CD44^{hi}) and central memory (CD62L^{hi}, CD44^{hi}) subsets of CD4$^+$ splenic T cells. **(I)** Total number of naïve, effector memory, and central memory CD4$^+$ subsets in the indicated genotypes. **(J**) IFN-γ and IL-2 abundance in serum at steady state. **(K)** The frequency of apoptotic (Annexin V-FITC$^+$) cells within CD4$^+$ T cell subsets in spleen and lymph nodes. **(L)** Mean fluorescence intensity (MFI) of Nur77 in naïve CD4$^+$ T cells in the spleen and lymph nodes. Black dots in graphs represent individual mice. Data were pooled from mice from at least three independent litters for a total of n = 3–13 mice per genotype. In (D, F, I), n=12 *Taok3*$^{+/+}$, n=7 *Taok3*$^{+/-}$, and n=12 *Taok3-/-* mice. In (G), n=9 *Taok3*$^{+/+}$, n=7 *Taok3*$^{+/-}$, and n=9 *Taok3*$^{-/-}$ mice. In (J), n=6 mice/genotype for IFN-γ, and n=13 *Taok3*$^{+/+}$

and n=10 *Taok3*$^{-/-}$ mice for IL-2. In (K), n=4 mice/genotype. In (L), n=3 mice/genotype. Error bars represent mean ± SEM. One-way ANOVA and Dunnett's multiple comparison. *p≤0.05, **p≤0.01, ***p≤0.001, ****p≤0.0001.

Fig. 2. Taok3 is required TCR sensitivity in naïve CD4$^+$ T cells but not for differentiation to effector cells. (A) Flow cytometric analysis of CFSE proliferation histograms of naïve CD4$^+$ T cells from *Taok3*$^{+/+}$, *Taok3*$^{+/-}$, or *Taok3*$^{-/-}$ mice stimulated ex vivo for 72h with 2μg/mL of CD3-specific antibody. **(B)** Bar plot showing daughter generation distributions from (A). **(C)** Mean fluorescence intensity (MFI) of CD69 in each daughter generation from (B)**. (D)** CFSE proliferation histograms of naïve CD4$^+$ T cells stimulated for 72h with 10μg/mL of CD3-specific antibody with or without exogenous IL-2. **(E)** Bar plot showing daughter generation distributions from (D). **(F)** Bar chart representing CD69 MFI in each daughter generation from (E). **(G)** Quantification of IL-2 produced by naïve CD4$^+$ T cells after 72h of stimulation with the indicated amounts of CD3-specific antibody, as measured by ELISA. **(H)** Bar chart representing the average MFI of IL-2Rα (CD25) in flow cytometric analysis of naïve CD4$^+$ T cells after 72h of stimulation with with as the indicated amounts of CD3 specific antibody . **(I)** IL-2 production curves in total CD4$^+$ T cells stimulated for 24 hours with various amounts of CD3-specific antibody. Data pooled from n=4 mice/genotype (A to F, H, J, K) or from n=3 mice/genotype (G and I). Error bars represent mean ± SEM. Statistical analysis: (B and E) $\chi 2$ tests were realized to compare the distribution of generations from the average of replicates from each genotype, (C, F, G, H) Two-way ANOVA and Dunnett's

multiple comparisons. (I) One-way ANOVAs versus *Taok3*$^{+/+}$ curve. *p≤0.05, **p≤0.01, ***p≤0.001, ****p≤0.0001.

Fig. 3. TAOK3 substitution mutants in the serine rich domain increaseIL-2 secretion upon TCR engagement. (A) Schematic representation of substitution mutations in TAOK3 vectors used for stable transduction and transfection. **(B)** Immunoblot blot analysis of V5-tagged TAOK3 mutant proteins within individual TAOK3 knockout (KO) Jurkat E6.1 cell lines expressing the TAOK3 constructs depicted in (A). Actin is a loading control. **(C)** Growth rate (% confluence/hour) and proliferation curves (% confluence over time) of TAOK3 KO Jurkat E6.1 cells with stable expression of the indicated TAOK3 constructs. **(D)** Flow cytometric analysis of CD3 and CD28 abundance in the indicated cell lines. **(E)** ELISA quantification of IL-2 production in the indicated cell lines stimulated with plate-bound CD3-specific antibody and soluble CD28-specific antibody. **(F)** ELISA quantification of IL-2 production by mouse primary $CD4^+$ T cells treated with DMSO (Vehicle), or various concentration of TAO kinase inhibitor (compound-43) and stimulated with immobilized CD3-specific antibody and soluble CD28-specific antibody for 24h or left unstimulated. Data pooled from three independent experiments (B to E) or mice (F). Error bars represent mean ± SEM. Statistical analysis: One-way ANOVA and Dunnett's multiple comparisons. *p≤0.05, **p≤0.01, ***p≤0.001, ****p≤0.0001.

Fig. 4. A T cell–specific increase in Shp-1 abundance and phosphatase activity desensitizes the TCR threshold of Taok3-deficient cells. (A) Immunoblot analysis of

phosphorylated (p) and total Lck, Zap-70, and Taok3 in mouse *Taok3*$^{+/+}$ or *Taok3*$^{-/-}$ CD4^{+} T cells stimulated with soluble CD3- and CD28-specific antibodies for 15 or 30 minutes or left unstimulated, resting (0). Total protein is used as the loading control. **(B)** Flow cytometric analysis of Ca^{2+} influx in naïve CD4^{+} T cells activated with CD3-specific antibody or Ionomycin. The bar chart shows the slope of the CD3 activation phase in *Taok3*$^{+/+}$ and *Taok3*$^{-/-}$ cells**. (C)** Immunoblot analysis and quantification of Shp-1 isolated (resting) CD4^{+} T cells from *Taok3*$^{+/+}$, *Taok3*$^{+/-}$, and *Taok3*$^{-/-}$ mice from multiple litters. Each data point represents one mouse. **(D)** *Shp-1* mRNA expression in total CD4^{+} T cells relative to housekeeping genes *Hprt* and *Hmbs* **(E)** Immunoblot analysis of SHP-1 protein after immunomagnetic separation of CD4^{+} T cells into a positive fraction (+) containing CD4^{+} T cells, and a negative fraction (-) containing splenocytes minus CD4^{+} T cells. The bar graph shows the amount of SHP-1 in each cell fraction (Normalized vs. CD4^{+}, Taok3$^{+/+}$). **(F)** XY plot showing mean fluorescence intensity of phosphorylated LCK (Tyr^{505}) in naïve CD4^{+} *Taok3*$^{+/+}$ or *Taok3*$^{-/-}$ T cells stimulated with immobilized CD3-specific antibody and soluble CD28-specific antibody for 5, 15 and 30 or left resting without stimulation. The abundance of phosphorylated Lck is relative to that in unstimulated/resting *Taok3*$^{+/+}$ T cells **(G)** Flow cytometric analysis of CD25^{+} cells and IL-2 production (ELISA) in wild type or knockout naïve CD4^{+} T cells treated with indicated concentrations of SHP-1 inhibitor NSC-87877 during the stimulation with immobilized CD3-specific antibody (5µg/mL) and soluble CD28-specific antibody (5µg/mL) for 48 hours. **(H)** Schematic representation of an iCRSPR mouse model used to induce the deletion of *Taok3* in T cells ex vivo. **(I)** Immunoblot blot analysis of phosphorylated and total Shp-1, Lck, Mek1/2, Erk1/2, Taok3, and Cas9 in T cells from *Taok3* iCRISPR mice

treated with vehicle or with doxycycline (Dox) to induce*Taok3* deletion. Vinculin is used as the loading control. **(J)** Quantification of IL-2 produced by vehicle-treated and *Taok3*-deleted total T cells after 24h and 96-hour of stimulation with CD3 and CD28 antibodies. **(K)** Flow cytometric analysis of IL-2Rα and IL-2Rβ (CD122) in vehicle-treated and *Taok3*-deleted total T cells. Data pooled from at least three independent experiments or biological replicates (mice). (B, J, and K) n=5 mice/genotype. (C) protein samples obtained from n=10 *Taok3*$^{+/+}$, n=4 *Taok3*$^{+/-}$, n=9 *Taok3*$^{-/-}$ mice were run independently six times. In (D) n=7 *Taok3*$^{+/+}$, n=2 *Taok3*$^{+/-}$, n=7 *Taok3*$^{-/-}$ mice. (E to G) n=3 mice/genotype. Error bars represent mean ± SEM. Statistical analysis: (C, D, F) One-way ANOVA with Dunnett's multiple comparison test. (F) One-way ANOVA (To assess TCR responsiveness vs. time). Two-way ANOVA and Dunnett's multiple comparison (E) or Šidák's multiple comparisons (F, G, J). (K) paired T-tests. *p≤0.05, **p≤0.01, ***p≤0.001, ****p≤0.0001.

Fig. 5. TAOK3 phosphorylates the PTP domain of SHP-1 at Thr^{394}. (A) Transfected TAOK3 was immunoprecipitated (IP) from HEK293T cells co-transfected with empty vector or FLAG-SHP1 with or without SRC^{Y527F}. TAOK3 immunoprecipitates and total cell lysates (Input) were immunoblotted for TAOK3, FLAG, and SRC. ACTIN is a loading control. **(B)** FLAG immunoprecipitates from HEK293T cells transfected with empty vector or SRC^{Y527F} plus wild-type (WT), C/S, or D/A mutant forms of SHP-1 were immunoblotted for TAOK3, FLAG, and SRC. **(C)** Endogenous TAOK3 was immunoprecipitated from lysates of Jurkat E6.1 cells that were either resting (0) or stimulated for 15 minutes with CD3 and CD28 antibodies. Immunoprecipitates were

blotted to show TAOK3 and SHP-1. GAPDH is a loading control. **(D)** Schematic representation of truncated SHP-1 mutants. **(E)** Immunoblotting for TAOK3 and FLAG in TAOK3 immunoprecipitates from HEK293T cells expressing wild-type TAOK3 and the indicated SHP-1 truncation mutants. **(F)** Schematic representation of incubation of FLAG-SHP-1 purified from HEK293T/17 cells i with and without purified recombinant TAOK3 (sino biological) for further detection of the phosphorylation site using mass spectrometry. The amino acid sequence above the tandem mass spectrum shows the region flanking SHP-1 Thr^{394} (red “t”). m/z is the mass/charge ratio. The “b”s and “y”s indicate mass spectrometry–identified fragment ions from the N-termini (b) and C-termini (y) from a phosphorylated Thr^{394} peptide in the SHP-1 + TAOK3 condition. **(G)** SHP-1–TAOK3 interaction model based on AlphaFold structures and experimentally defined interaction sites. For SHP-1, Thr^{394} is shown in magenta, the PTP domain in orange, the SH2 domains in green, and the, C-terminus in red. For TAOK3, the kinase domain is shown in blue and the coiled-coiled domain in grey. (A-E) Data are representative of at least three independent experiments.

Fig. 6. TAOK3 modulates SHP-1 protein-protein interactions and its ubiquitin-dependent proteasomal degradation. (A to D) Affinity-capture mass spectrometry of lysates of HEK293T/17 cells transfected with the indicated combinations of SHP-1, TAOK3, and SRC^{Y527F}. (A) Venn diagrams showing the number of specific co-interactors having differential abundance between the condition groups (FDR<0.5). (B) Dot plot of the differentially enriched or diminished co-interactors from A. (FDR<0.5). (C) Protein interaction network for the significantly enriched co-interactors in the SHP-1 +

TAOK3 condition and associated molecular function from (B). (D) Bar plot of the significantly enriched/diminished molecular functions from (B). **(E)** Immunoblot analysis of TAOK3 and SHP-1 in Jurkat T cells for which overexpression of TAOK3 is controlled by a TET-ON system (doxycycline-inducible). Total protein is used as the loading control. **(F)** Immunoblotting for HA, FLAG, and TAOK3 in total cell lysates (Input) and FLAG immunoprecipitates (IP) in HEK293T/17 cells expressing HA-Ubiquitin, FLAG-SHP-1, and TAOK3 and treated with or without MG-132 proteasome inhibitor as indicated. Actin is used as the loading control. **(G)** Immunoblotting for HA and FLAG in FLAG immunoprecipitates from HEK293T/17 cells expressing HA-Ubiquitin, TAOK3, and FLAG-tagged wild-type (WT) or mutant (T394A=T/A, T394D=T/D) SHP-1 as indicated and treated with MG-132. **(H)** Immunoblot analysis of SHP-1, SHP-2, and TAOK3 in Jurkat E6.1 cells subjected to CD3 and CD28 stimulation and/or treatment with Cycloheximide as indicated. GAPDH was used as the loading control. (E-H) Data are representative of at least three independent experiments.

Fig. 7. Model for TAOK3-mediated SHP-1 degradation and regulation of TCR signaling. SHP-1 inhibits the activation of the TCR signaling cascade by dephosphorylating LCK ,ZAP-70 and the ITAMs in the intracellular chains of the TCR complex. In the context of TCR signaling, TAOK3 interacts with SHP-1 and mediates its phosphorylation at Thr^{394}. This leads to mono- and polyubiquitylation of SHP-1, which in turn promotes its proteasomal degradation. TAOK3 therefore reduces the stability of SHP-1, thereby increasing the sensitivity of T cells to activation.

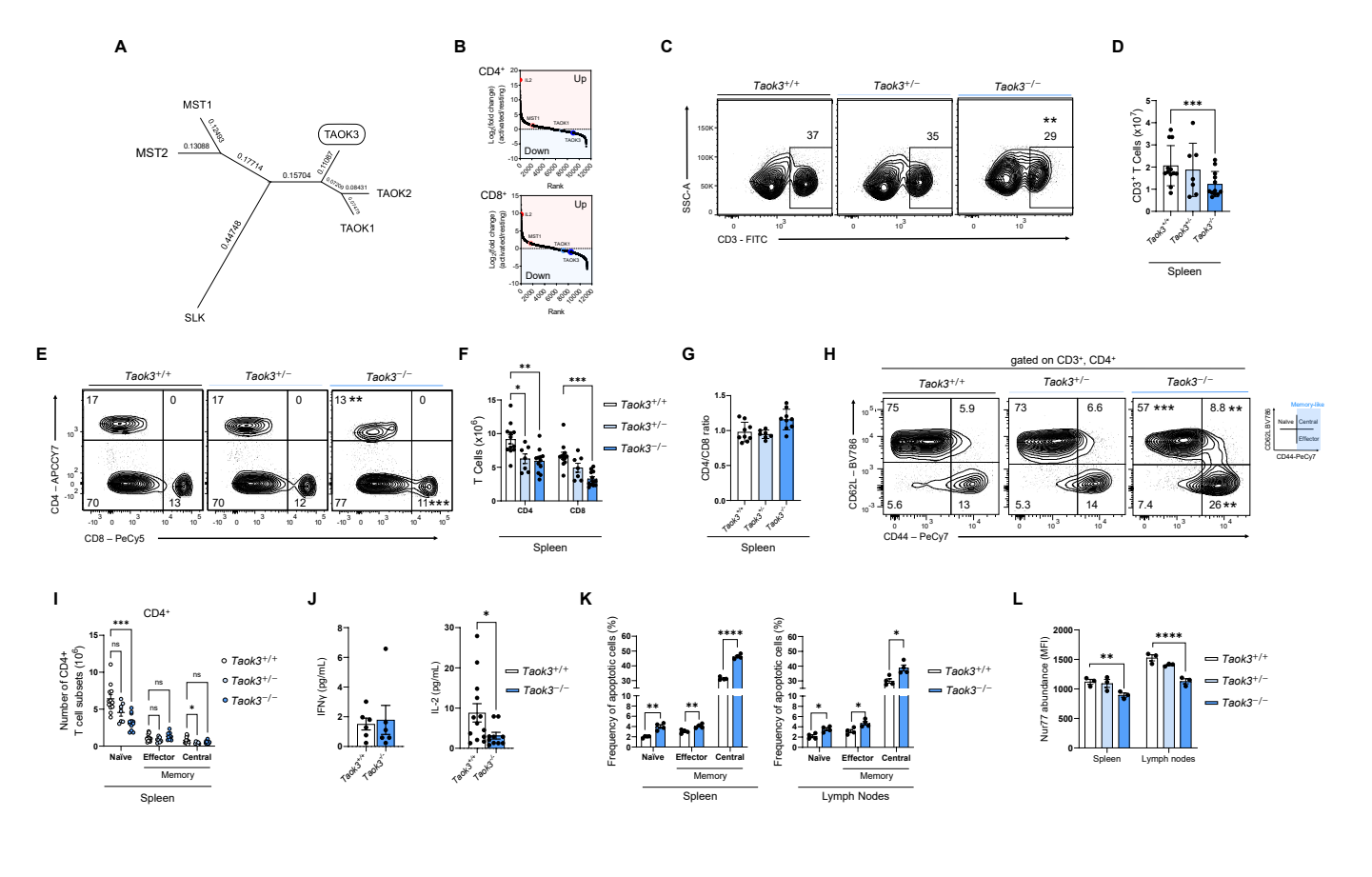
A
MST1
MST2
TAOK3
TAOK2
TAOK1
SLK
0.13088
0.12493
0.17714
0.15704
0.11097
0.10259
0.08431
0.12121
0.44748
B
CD4+
CD8+
Up
Down
Log2fold change (activated/resting)
Rank
IL2
MST1
TAOK3
TAOK2
C
Taok3+/+
Taok3+/−
Taok3−/−
SSC-A
CD3 - FITC
37
35
29
D
CD3+ T Cells (x10^7)
Spleen
E
CD4 – APCCY7
CD8 – PeCy5
17
0
70
13
12
11
F
T Cells (x10^6)
CD4
CD8
Spleen
G
CD4/CD8 ratio
Spleen
H
gated on CD3+, CD4+
CD62L – BV786
CD44 – PeCy7
75
5.9
5.6
73
6.6
5.3
14
57
8.8
7.4
26
Memory-like
Naive
Central
Effector
I
CD4+
Number of CD4+ T cell subsets (10^6)
Naive
Effector
Central
Memory
Spleen
J
IFNγ (pg/mL)
IL-2 (pg/mL)
K
Frequency of apoptotic cells (%)
Spleen
Lymph Nodes
L
Nur77 abundance (MFI)
Spleen
Lymph nodes

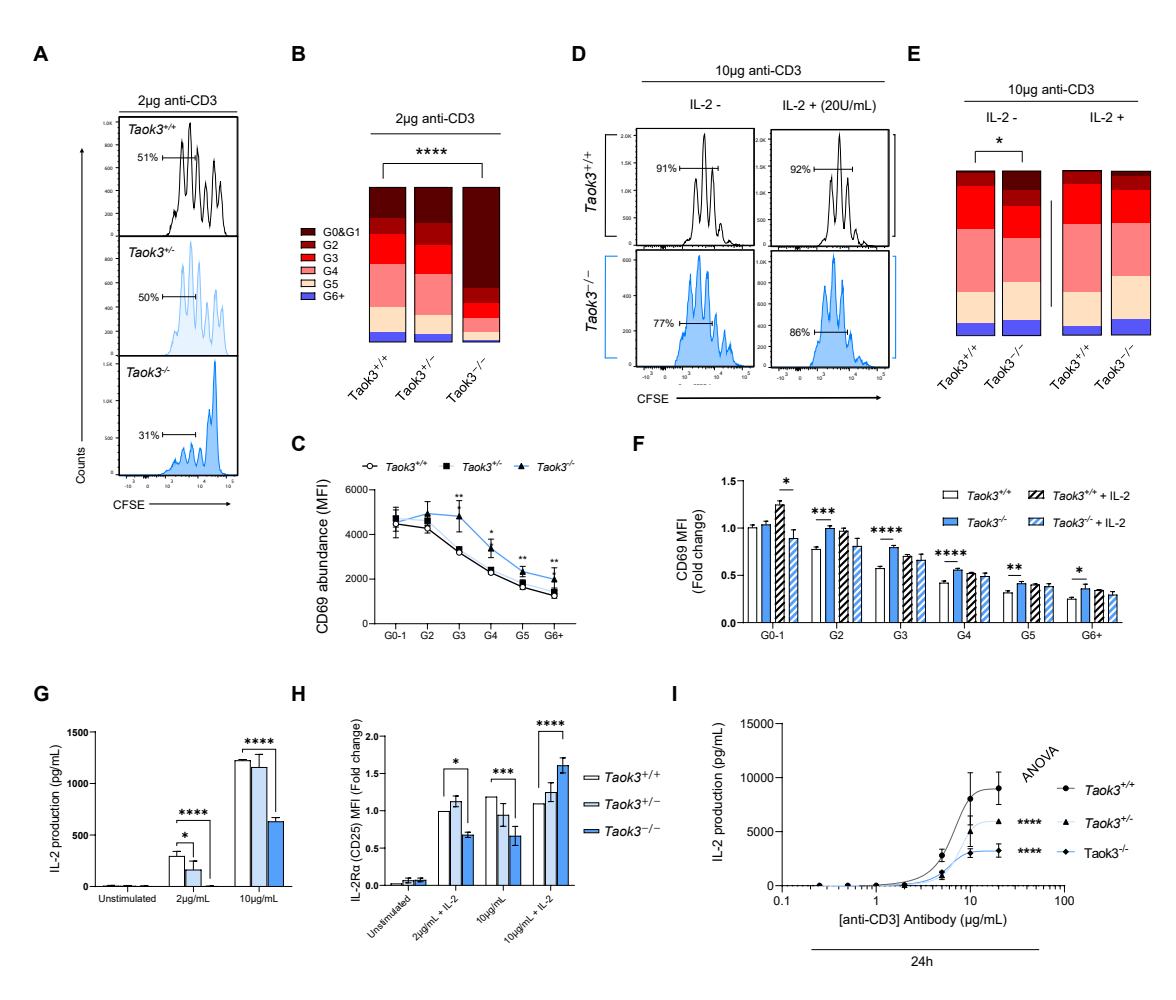
A
2μg anti-CD3
Taok3+/+
51%
Taok3+/-
50%
Taok3-/-
31%
Counts
CFSE
B
2μg anti-CD3
****
G0&G1
G2
G3
G4
G5
G6+
Taok3+/+
Taok3+/-
Taok3-/-
C
Taok3+/+
Taok3+/-
Taok3-/-
CD69 abundance (MFI)
G0-1
G2
G3
G4
G5
G6+
D
10μg anti-CD3
IL-2 -
IL-2 + (20U/mL)
Taok3+/+
91%
92%
Taok3-/-
77%
86%
CFSE
E
10μg anti-CD3
IL-2 -
IL-2 +
*
Taok3+/+
Taok3-/-
Taok3+/+
Taok3-/-
F
CD69 MFI (Fold change)
Taok3+/+
Taok3-/-
Taok3+/+ + IL-2
Taok3-/- + IL-2
G0-1
G2
G3
G4
G5
G6+
G
IL-2 production (pg/mL)
Unstimulated
2μg/mL
10μg/mL
H
IL-2Rα (CD25) MFI (Fold change)
Unstimulated
2μg/mL + IL-2
10μg/mL
10μg/mL + IL-2
Taok3+/+
Taok3+/-
Taok3-/-
I
IL-2 production (pg/mL)
ANOVA
Taok3+/+
Taok3+/-
Taok3-/-
[anti-CD3] Antibody (μg/mL)
24h

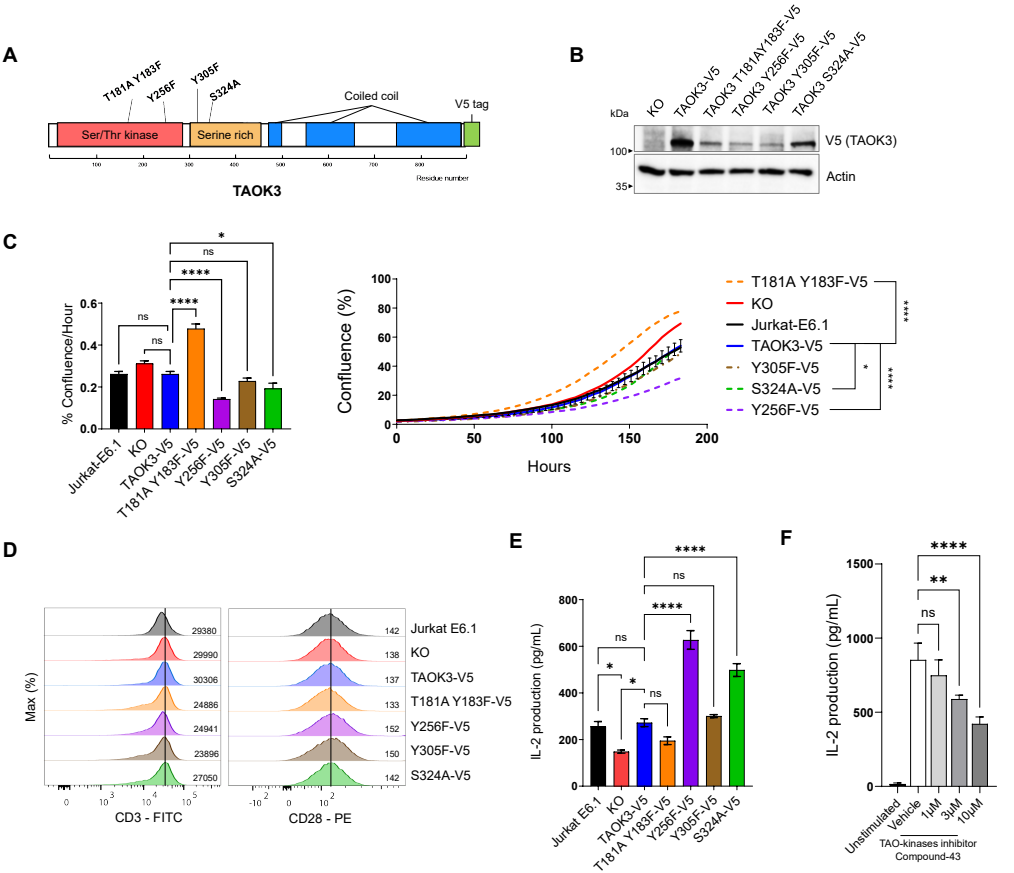
A
T181A Y183F
Y256F
Y305F
S324A
Coiled coil
V5 tag
Ser/Thr kinase
Serine rich
Residue number
TAOK3
B
kDa
KO
TAOK3-V5
TAOK3 T181AY183F-V5
TAOK3 Y256F-V5
TAOK3 Y305F-V5
TAOK3 S324A-V5
100
35
V5 (TAOK3)
Actin
C
% Confluence/Hour
Jurkat-E6.1
KO
TAOK3-V5
T181A Y183F-V5
Y256F-V5
Y305F-V5
S324A-V5
Confluence (%)
Hours
D
Max (%)
29380
29990
30306
24886
24941
23896
27050
142
138
137
133
152
150
142
Jurkat E6.1
KO
TAOK3-V5
T181A Y183F-V5
Y256F-V5
Y305F-V5
S324A-V5
CD3 - FITC
CD28 - PE
E
IL-2 production (pg/mL)
F
IL-2 production (pg/mL)
Unstimulated
Vehicle
1μM
3μM
10μM
TAO-kinases inhibitor
Compound-43

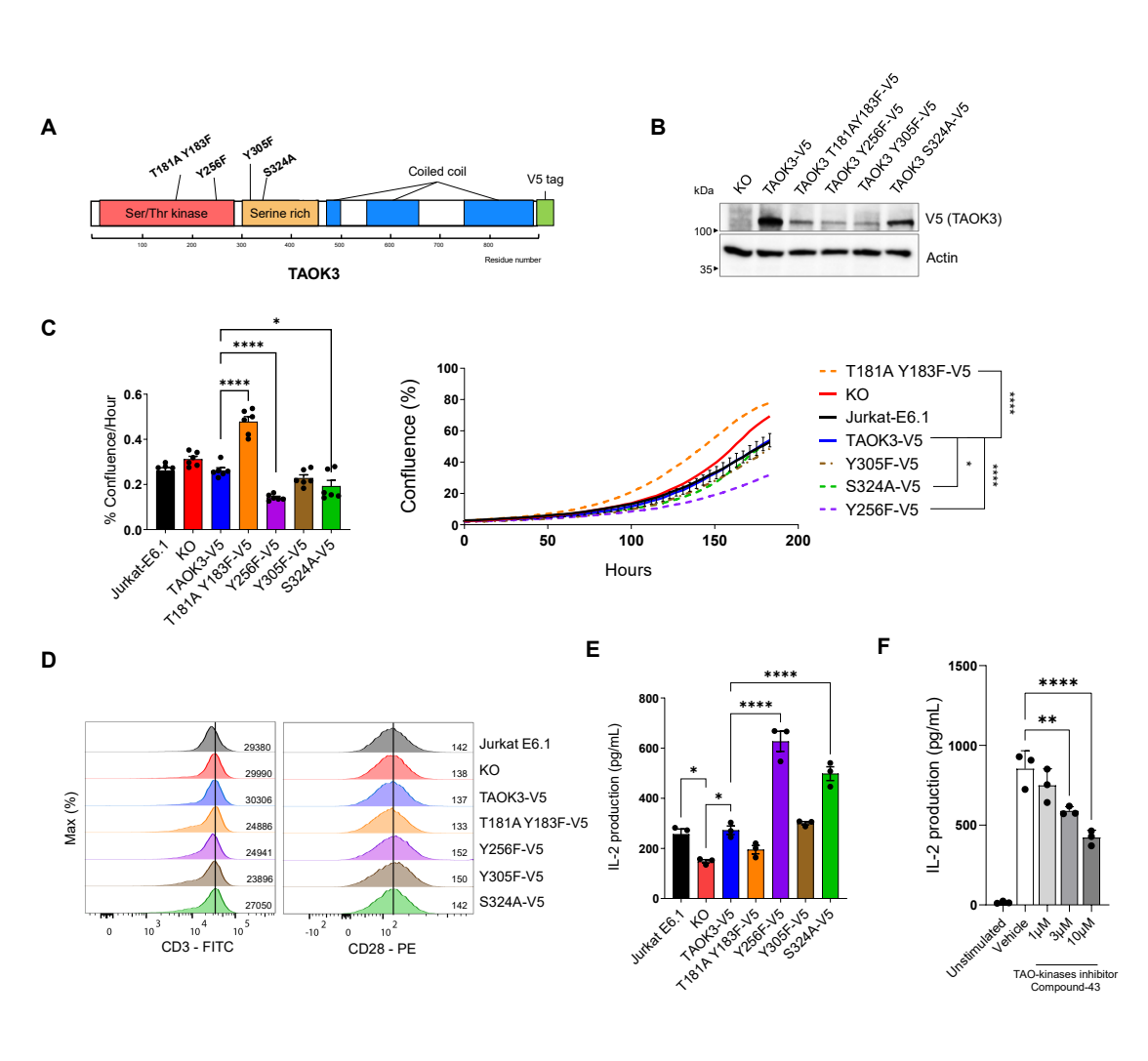
A
T181A Y183F
Y256F
Y305F
S324A
Coiled coil
V5 tag
Ser/Thr kinase
Serine rich
100
200
300
400
500
600
700
800
Residue number
TAOK3
B
kDa
KO
TAOK3-V5
TAOK3 T181AY183F-V5
TAOK3 Y256F-V5
TAOK3 Y305F-V5
TAOK3 S324A-V5
100
35
V5 (TAOK3)
Actin
C
% Confluence/Hour
0.0
0.2
0.4
0.6
****
****
*
Jurkat-E6.1
KO
TAOK3-V5
T181A Y183F-V5
Y256F-V5
Y305F-V5
S324A-V5
Confluence (%)
0
20
40
60
80
100
0
50
100
150
200
Hours
T181A Y183F-V5
KO
Jurkat-E6.1
TAOK3-V5
Y305F-V5
S324A-V5
Y256F-V5
****
*
****
D
Max (%)
29380
29990
30306
24886
24941
23896
27050
142
138
137
133
152
150
142
Jurkat E6.1
KO
TAOK3-V5
T181A Y183F-V5
Y256F-V5
Y305F-V5
S324A-V5
CD3 - FITC
CD28 - PE
E
IL-2 production (pg/mL)
0
200
400
600
800
*
*
****
****
Jurkat E6.1
KO
TAOK3-V5
T181A Y183F-V5
Y256F-V5
Y305F-V5
S324A-V5
F
IL-2 production (pg/mL)
0
500
1000
1500
****
**
Unstimulated
Vehicle
1μM
3μM
10μM
TAO-kinases inhibitor
Compound-43

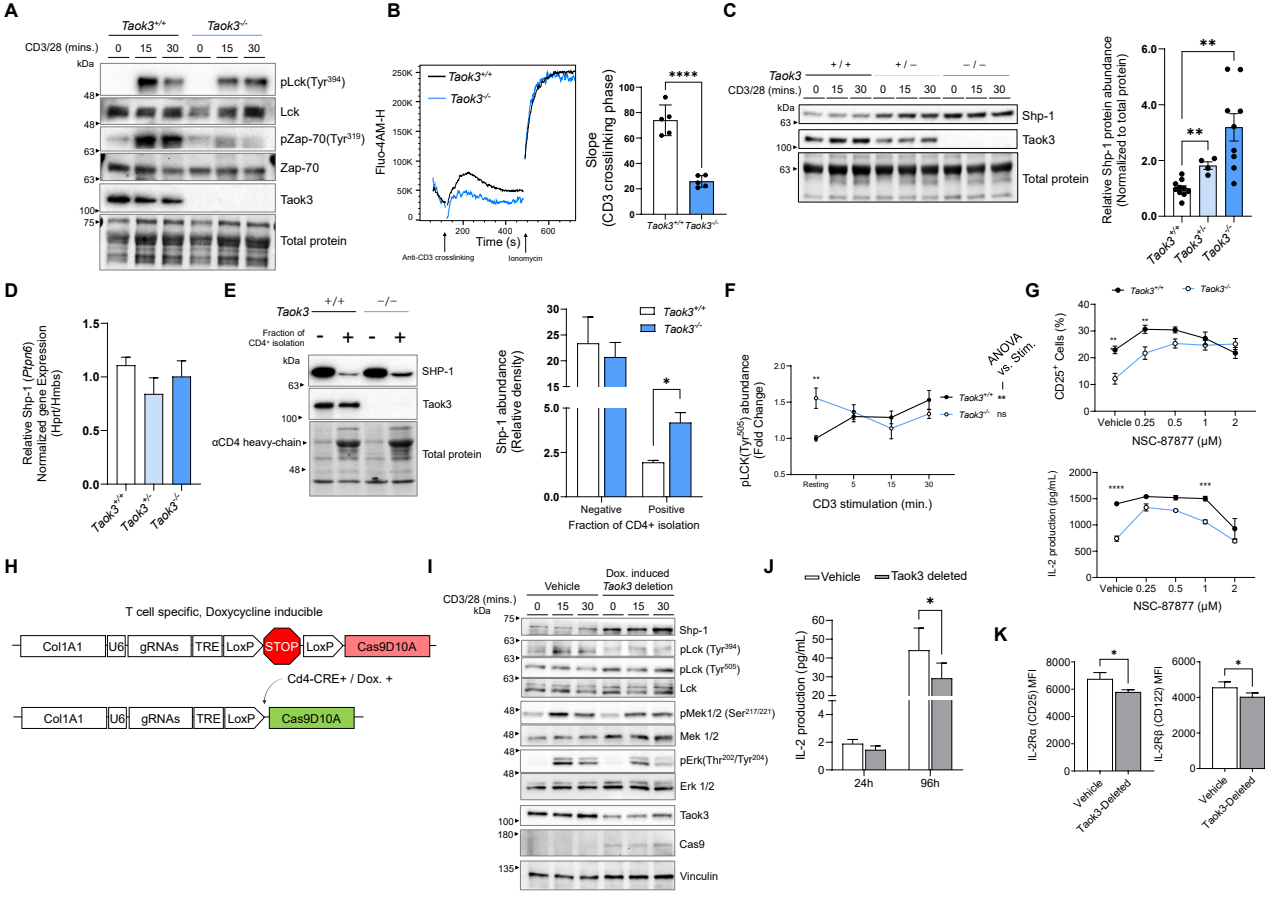
A
Taok3+/+
Taok3−/−
CD3/28 (mins.)
0 15 30 0 15 30
kDa
pLck(Tyr394)
Lck
pZap-70(Tyr319)
Zap-70
Taok3
Total protein
B
Taok3+/+
Taok3−/−
Fluo-4AM-H
Time (s)
Anti-CD3 crosslinking
Ionomycin
Slope (CD3 crosslinking phase)
****
C
Taok3
+ / +
+ / −
− / −
CD3/28 (mins.)
Shp-1
Taok3
Total protein
Relative Shp-1 protein abundance (Normalized to total protein)
D
Relative Shp-1 (Ptpn6) Normalized gene Expression (Hprt/Hmbs)
E
Taok3
+/+
−/−
Fraction of CD4+ isolation
SHP-1
Taok3
αCD4 heavy-chain
Total protein
Shp-1 abundance (Relative density)
Negative
Positive
Fraction of CD4+ isolation
F
pLCK(Tyr505) abundance (Fold Change)
Resting
CD3 stimulation (min.)
ANOVA vs. Stim.
G
CD25+ Cells (%)
NSC-87877 (μM)
IL-2 production (pg/mL)
H
T cell specific, Doxycycline inducible
Col1A1
U6
gRNAs
TRE
LoxP
STOP
Cas9D10A
Cd4-CRE+ / Dox. +
I
Vehicle
Dox. induced Taok3 deletion
CD3/28 (mins.)
Shp-1
pLck (Tyr394)
pLck (Tyr505)
Lck
pMek1/2 (Ser217/221)
Mek 1/2
pErk(Thr202/Tyr204)
Erk 1/2
Taok3
Cas9
Vinculin
J
Vehicle
Taok3 deleted
IL-2 production (pg/mL)
24h
96h
K
IL-2Rα (CD25) MFI
IL-2Rβ (CD122) MFI
Vehicle
Taok3-Deleted

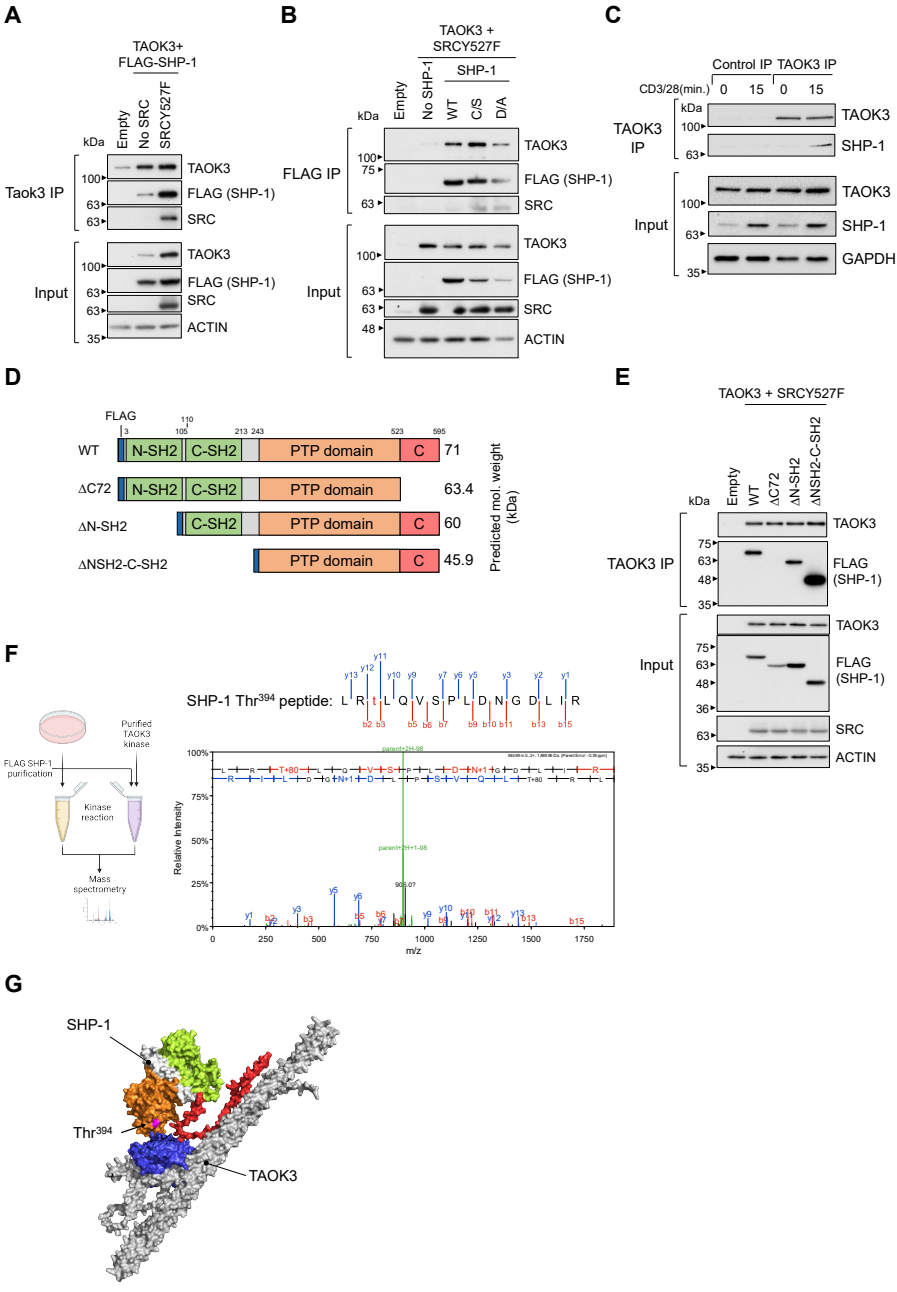
A
TAOK3+
FLAG-SHP-1
Empty
No SRC
SRCY527F
kDa
Taok3 IP
TAOK3
FLAG (SHP-1)
SRC
Input
TAOK3
FLAG (SHP-1)
SRC
ACTIN
B
TAOK3 +
SRCY527F
SHP-1
Empty
No SHP-1
WT
C/S
D/A
kDa
FLAG IP
TAOK3
FLAG (SHP-1)
SRC
Input
TAOK3
FLAG (SHP-1)
SRC
ACTIN
C
Control IP
TAOK3 IP
CD3/28(min.)
0
15
0
15
kDa
TAOK3 IP
TAOK3
SHP-1
Input
TAOK3
SHP-1
GAPDH
D
FLAG
WT
N-SH2
C-SH2
PTP domain
C
71
ΔC72
63.4
ΔN-SH2
60
ΔNSH2-C-SH2
45.9
Predicted mol. weight (kDa)
E
TAOK3 + SRCY527F
Empty
WT
ΔC72
ΔN-SH2
ΔNSH2-C-SH2
kDa
TAOK3 IP
TAOK3
FLAG (SHP-1)
Input
TAOK3
FLAG (SHP-1)
SRC
ACTIN
F
Purified TAOK3 kinase
FLAG SHP-1 purification
Kinase reaction
Mass spectrometry
SHP-1 Thr394 peptide: L R t L Q V S P L D N G D L I R
Relative Intensity
m/z
G
SHP-1
Thr394
TAOK3

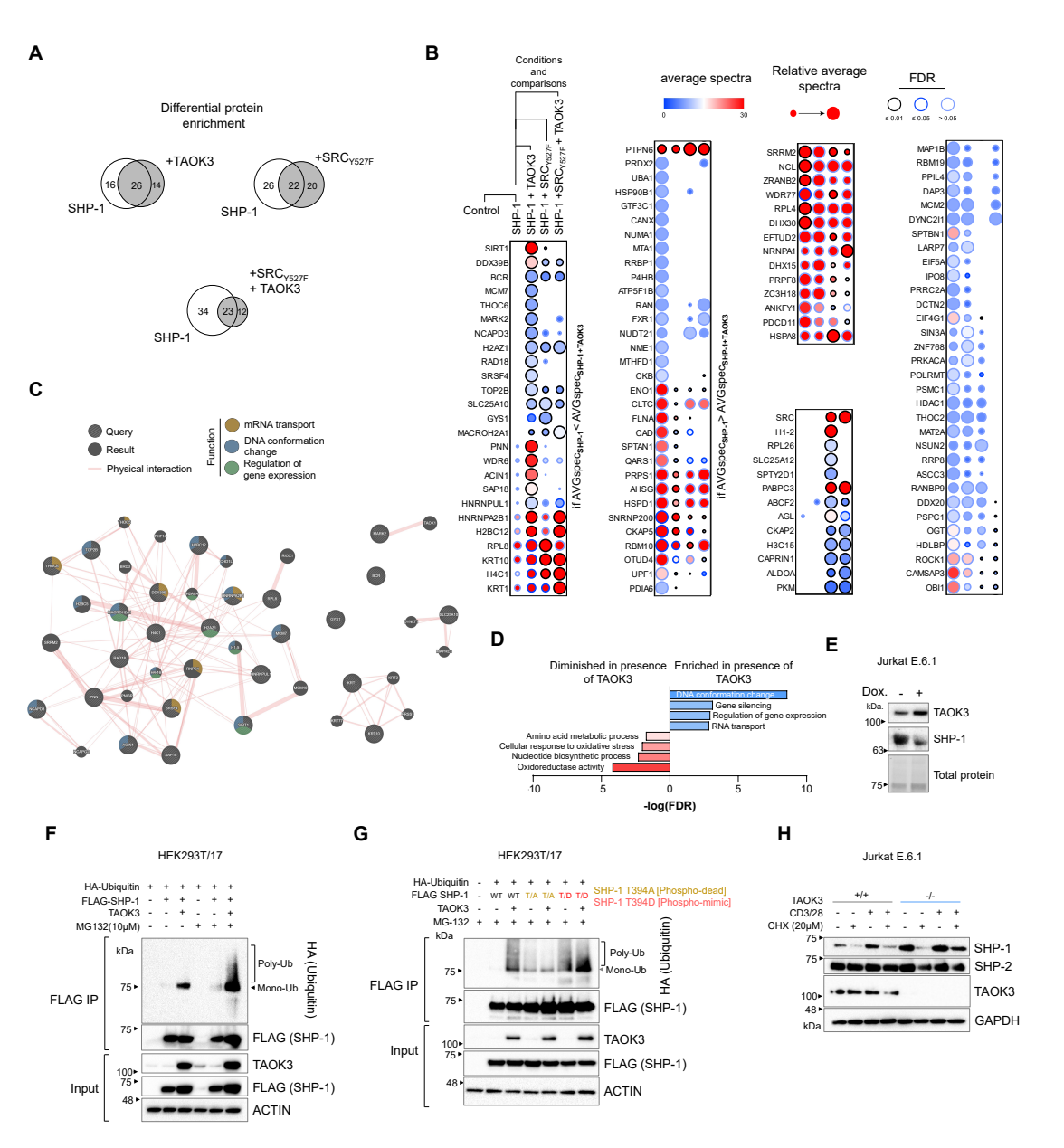
A
Differential protein enrichment
+TAOK3
SHP-1
16
26
14
+SRCY527F
SHP-1
26
22
20
+SRCY527F + TAOK3
SHP-1
34
23
12
B
Conditions and comparisons
Control
SHP-1
SHP-1 + TAOK3
SHP-1 + SRCY527F
SHP-1 +SRCY527F + TAOK3
average spectra
0
30
Relative average spectra
FDR
≤ 0.01
≤ 0.05
> 0.05
SIRT1
DDX39B
BCR
MCM7
THOC6
MARK2
NCAPD3
H2AZ1
RAD18
SRSF4
TOP2B
SLC25A10
GYS1
MACROH2A1
PNN
WDR6
ACIN1
SAP18
HNRNPUL1
HNRNPA2B1
H2BC12
RPL8
KRT10
H4C1
KRT1
if AVGspecSHP-1 < AVGspecSHP-1+TAOK3
PTPN6
PRDX2
UBA1
HSP90B1
GTF3C1
CANX
NUMA1
MTA1
RRBP1
P4HB
ATP5F1B
RAN
FXR1
NUDT21
NME1
MTHFD1
CKB
ENO1
CLTC
FLNA
CAD
SPTAN1
QARS1
PRPS1
AHSG
HSPD1
SNRNP200
CKAP5
RBM10
OTUD4
UPF1
PDIA6
if AVGspecSHP-1 > AVGspecSHP-1+TAOK3
SRRM2
NCL
ZRANB2
WDR77
RPL4
DHX30
EFTUD2
NRNPA1
DHX15
PRPF8
ZC3H18
ANKFY1
PDCD11
HSPA8
SRC
H1-2
RPL26
SLC25A12
SPTY2D1
PABPC3
ABCF2
AGL
CKAP2
H3C15
CAPRIN1
ALDOA
PKM
MAP1B
RBM19
PPIL4
DAP3
MCM2
DYNC2I1
SPTBN1
LARP7
EIF5A
IPO8
PRRC2A
DCTN2
EIF4G1
SIN3A
ZNF768
PRKACA
POLRMT
PSMC1
HDAC1
THOC2
MAT2A
NSUN2
RRP8
ASCC3
RANBP9
DDX20
PSPC1
OGT
HDLBP
ROCK1
CAMSAP3
OBI1
C
Query
Result
Physical interaction
Function
mRNA transport
DNA conformation change
Regulation of gene expression
D
Diminished in presence of TAOK3
Enriched in presence of TAOK3
DNA conformation change
Gene silencing
Regulation of gene expression
RNA transport
Amino acid metabolic process
Cellular response to oxidative stress
Nucleotide biosynthetic process
Oxidoreductase activity
10
5
0
5
10
-log(FDR)
E
Jurkat E.6.1
Dox. - +
kDa.
100
63
75
TAOK3
SHP-1
Total protein
F
HEK293T/17
HA-Ubiquitin + + + + + +
FLAG-SHP-1 - + + - + +
TAOK3 - - + - - +
MG132(10μM) - - - + + +
kDa
75
75
Poly-Ub
Mono-Ub
HA (Ubiquitin)
FLAG IP
FLAG (SHP-1)
100
75
48
TAOK3
FLAG (SHP-1)
ACTIN
Input
G
HEK293T/17
HA-Ubiquitin - + + + + + +
FLAG SHP-1 - WT WT T/A T/A T/D T/D
SHP-1 T394A [Phospho-dead]
SHP-1 T394D [Phospho-mimic]
TAOK3 - - + - + - +
MG-132 + + + + + + +
kDa
75
75
Poly-Ub
Mono-Ub
HA (Ubiquitin)
FLAG IP
FLAG (SHP-1)
100
75
48
TAOK3
FLAG (SHP-1)
ACTIN
Input
H
Jurkat E.6.1
TAOK3 +/+ -/-
CD3/28 - + + + - + +
CHX (20μM) - + - + - + -
75
75
SHP-1
SHP-2
100
48
TAOK3
GAPDH
kDa

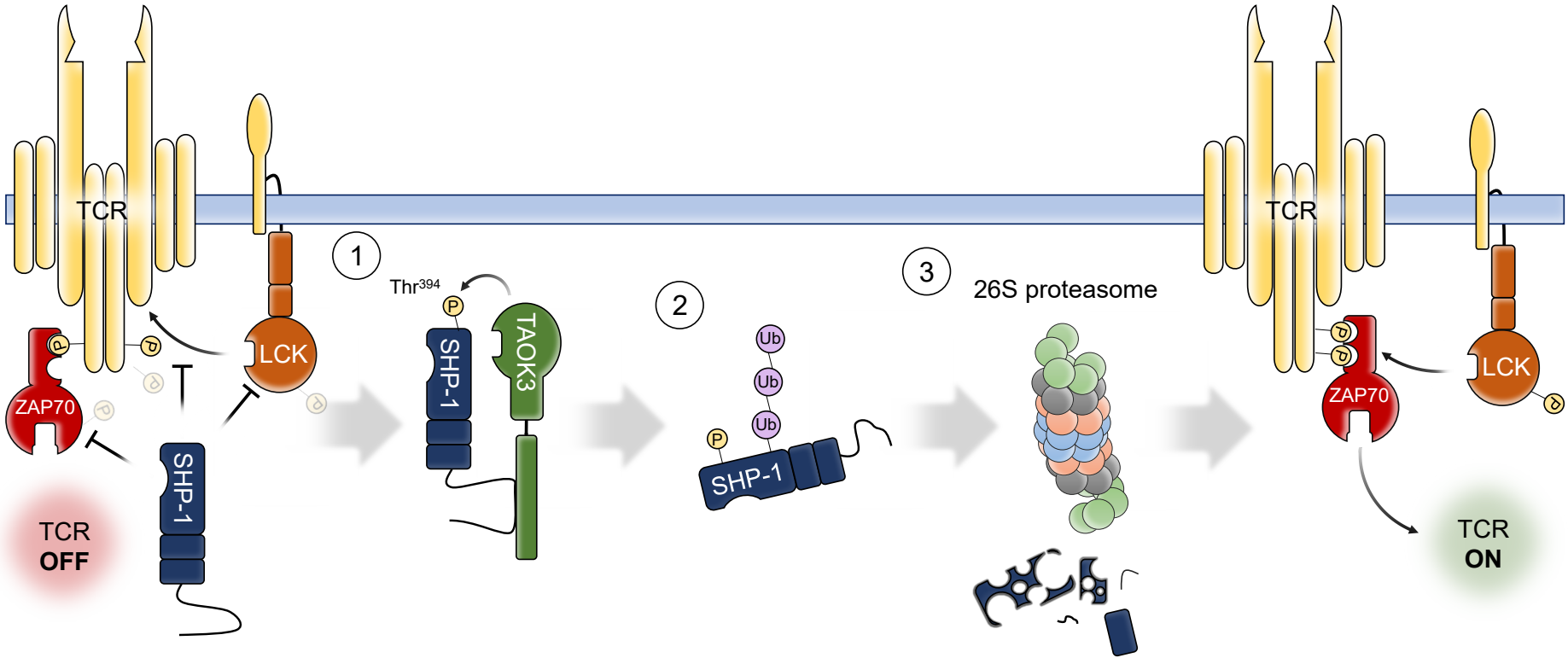
TCR
LCK
ZAP70
SHP-1
TCR
OFF
1
Thr394
P
SHP-1
TAOK3
2
Ub
Ub
Ub
P
SHP-1
3
26S proteasome
TCR
LCK
ZAP70
TCR
ON

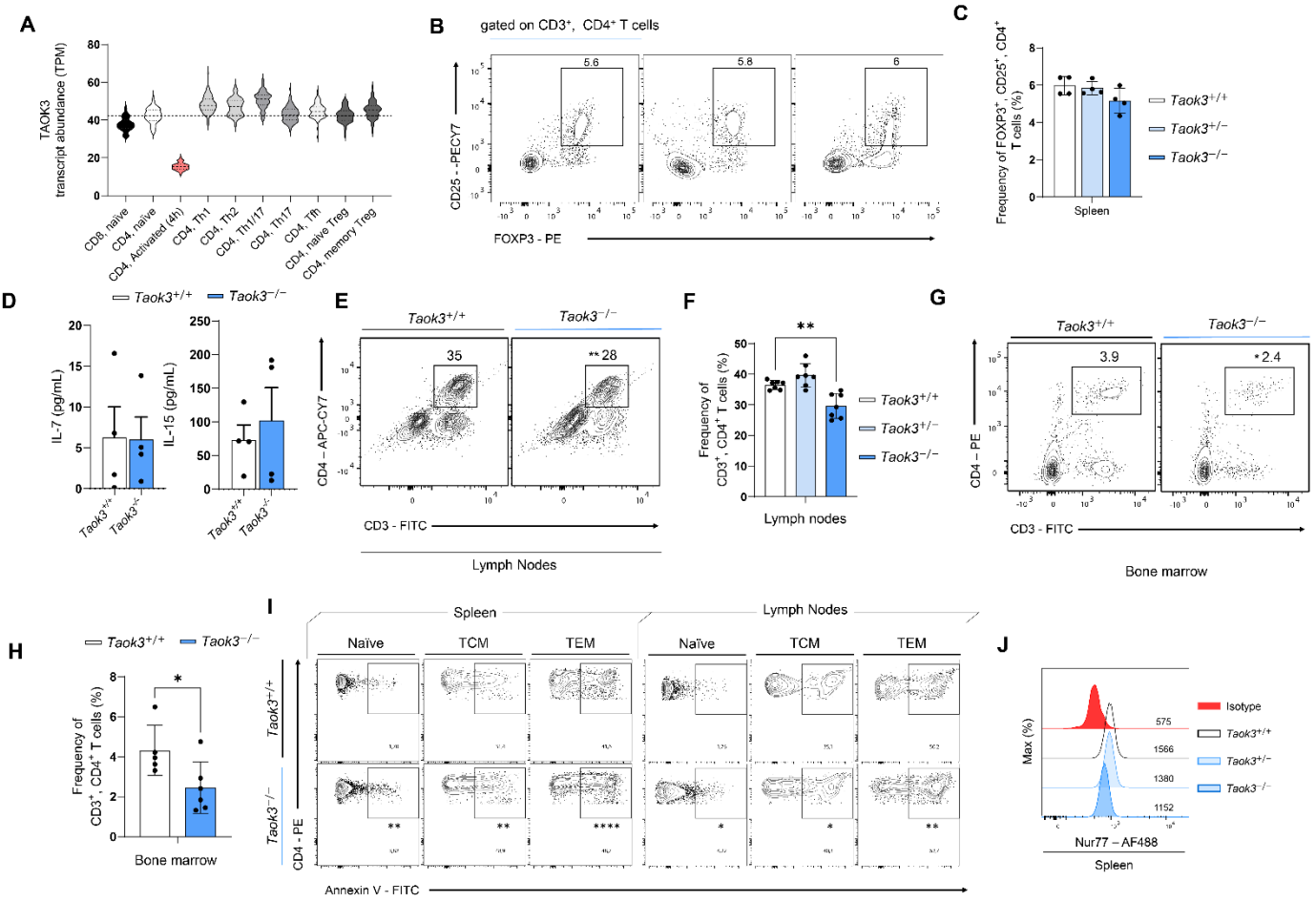

Fig. S1. Supplemental mouse immunophenotyping. These data complement Fig. 1. (**A**) Expression abundance analyses using data extracted from the Database of Immune Cell Expression (DICE). Violin plot represents the relative *TAOK3* transcript abundance in various T cell subsets. (**B**) Gating strategy used to identify FOXP3$^+$, CD25$^+$ T-reg cells. (**C**) Bar chart representing the frequency of FOXP3$^+$, CD25$^+$ population within the CD3$^+$, CD4$^+$ population in the spleen. (**D**) Serum IL-7 and IL-15 amounts in *Taok3*$^{+/+}$ and *Taok3*$^{-/-}$ mice. **(E)** Gating strategy used to define CD3$^+$, CD4$^+$ T cells isolated from lymph nodes (pooled Axillary and Inguinal). **(F)** Bar chart representing the frequency of CD3$^+$, CD4$^+$ population in lymph nodes. **(G)** Gating strategy used to define CD3$^+$, CD4$^+$ T cells isolated from bone marrow. **(H)** Bar chart representing the frequency of CD3$^+$, CD4$^+$ population in lymph nodes bone marrow. **(I)** Flow cytometry plots for the quantification of apoptotic Annexin V$^+$ Naïve (CD62L$^+$, CD44$^-$), T central memory (TCM, CD62$^+$, CD44$^+$), or T effector memory (TEM, CD62$^-$, CD44$^+$) CD4$^+$ T cells. **(J)** Flow cytometric analysis of Nur77 in splenic CD4+ Naïve T cells (from Fig. 1L). Black dots represent individual mice. Error bars represent mean ± SEM. Data pooled from least three independent biological replicates for a total of (B, C, D, I) n=4 mice/genotype, (E and F) n=7 mice/genotype, (G and H) n=5 mice/genotype, and (J) n=3 mice/genotype. Statistical analysis: (C and F) One-way ANOVA and Dunnett's multiple comparisons; (D and H) Unpaired T-test. *$P \leq 0.05$, **$P \leq 0.01$, ***$P \leq 0.001$, ****$P \leq 0.000$.

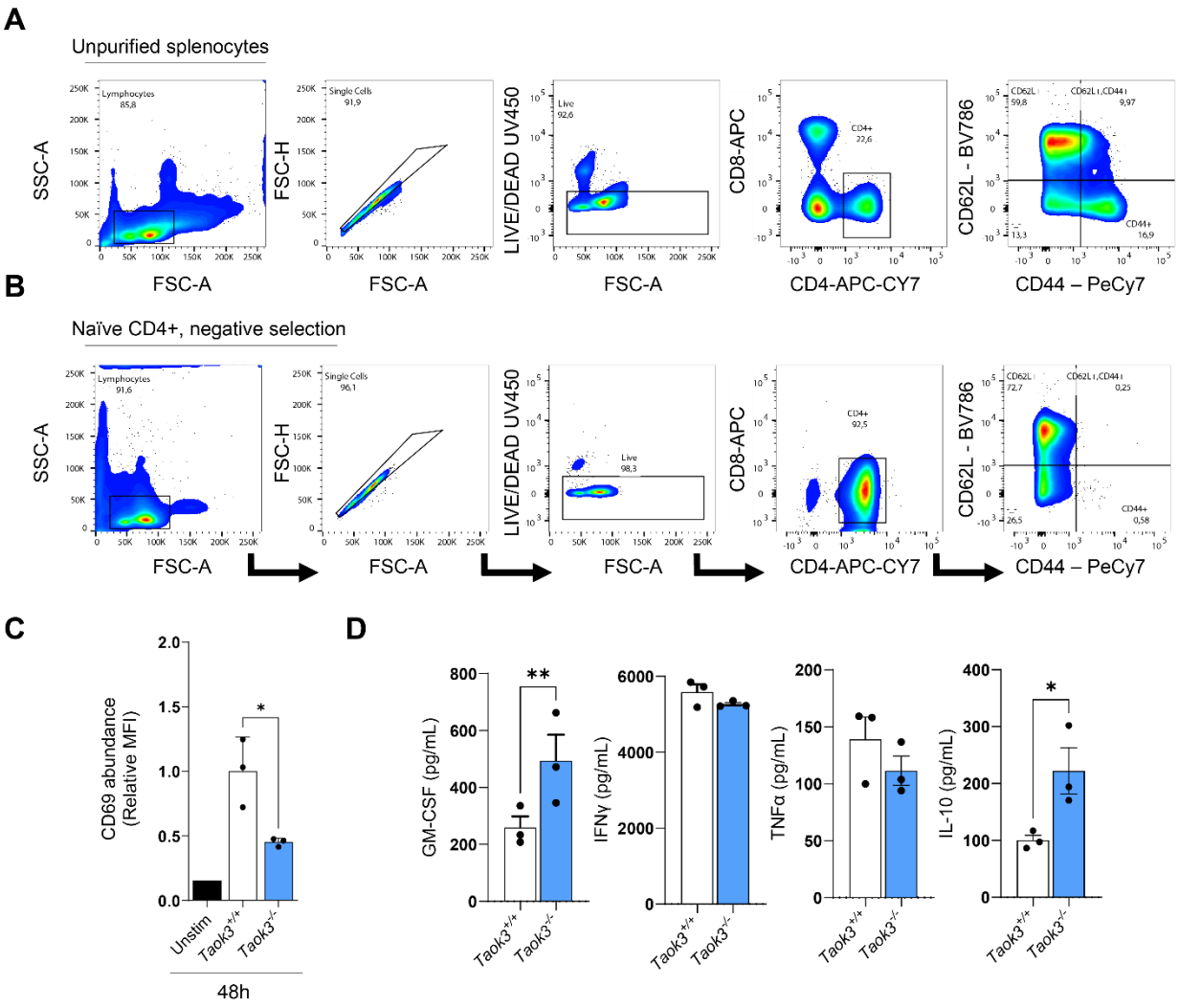

Fig. S2. Additional data relating to Fig. 2. (**A** and **B**) Gating strategy used to confirm proper isolation of naïve $CD4^+$ T cells. Sorting of total splenocytes before isolation (A) and naïve $CD4^+$ isolated splenocytes (B) are shown. (**C**) CD69 abundance in naïve $CD4^+$ T cells stimulated with CD3 and CD28 for 48 hours. (**D**) Cytokine multiplex analysis of GM-CSF, IFN-γ, TNF-α, and IL-10 in total T cells stimulated with CD3 and CD28 for 24 hours. (C and D) Data pooled from at least three biological replicates (mice). Error bars represent mean ± SEM. black dots representing individual mice. (C and D) n=3 mice/genotype. Statistical analysis: (C) One-way ANOVA and Dunnett's multiple comparisons; (D) Paired T-tests. *p≤0.05, **p≤0.01, ***p≤0.001, ****p≤0.000.

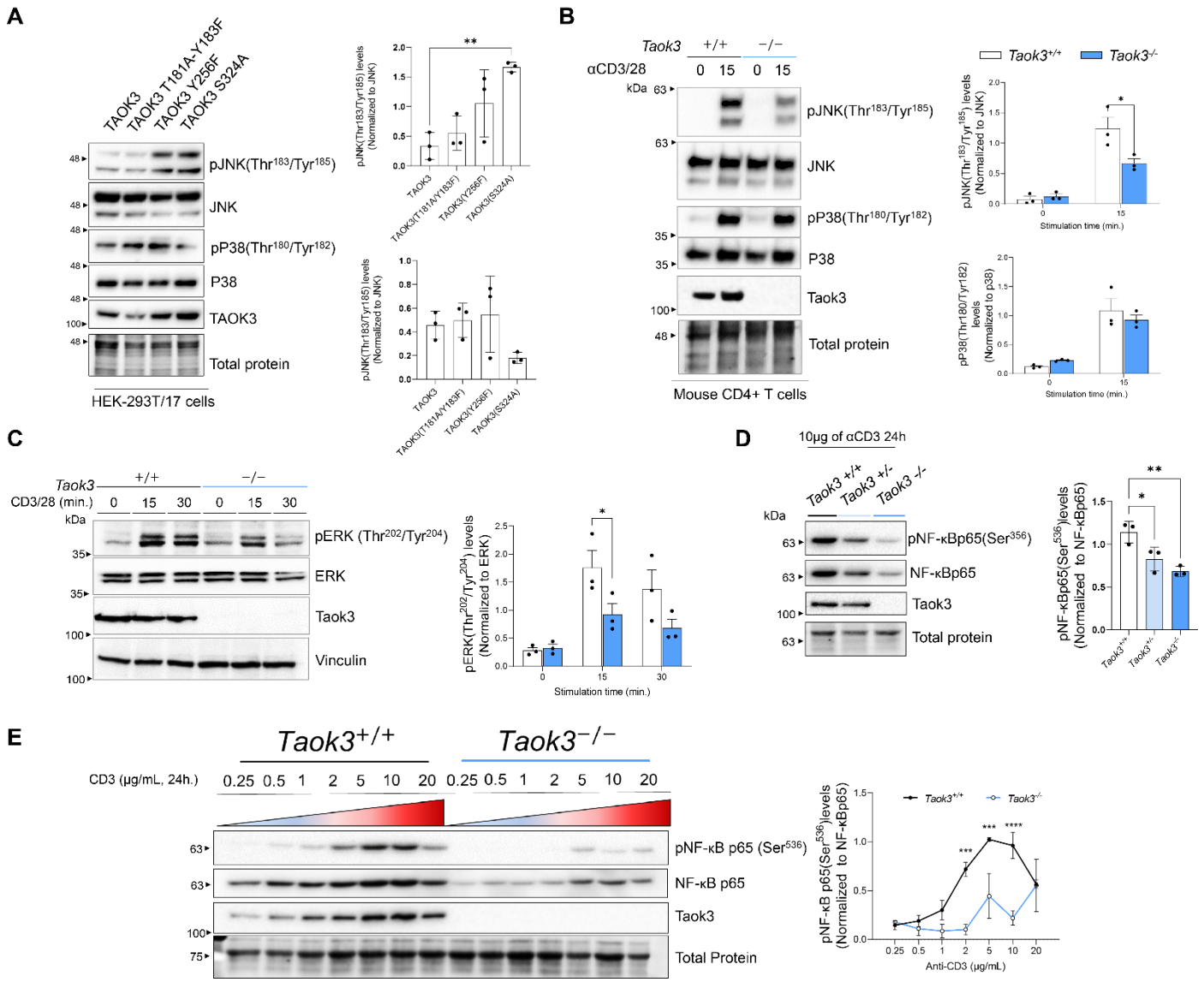
A
TAOK3
TAOK3 T181A-Y183F
TAOK3 Y256F
TAOK3 S324A
pJNK(Thr183/Tyr185)
JNK
pP38(Thr180/Tyr182)
P38
TAOK3
Total protein
HEK-293T/17 cells
pJNK(Thr183/Tyr185) levels (Normalized to JNK)
TAOK3
TAOK3(T181A/Y183F)
TAOK3(Y256F)
TAOK3(S324A)
B
Taok3 +/+ −/−
αCD3/28 0 15 0 15
kDa
pJNK(Thr183/Tyr185)
JNK
pP38(Thr180/Tyr182)
P38
Taok3
Total protein
Mouse CD4+ T cells
Taok3+/+
Taok3-/-
pJNK(Thr183/Tyr185) levels (Normalized to JNK)
Stimulation time (min.)
pP38(Thr180/Tyr182) levels (Normalized to p38)
C
Taok3 +/+ −/−
CD3/28 (min.) 0 15 30 0 15 30
kDa
pERK (Thr202/Tyr204)
ERK
Taok3
Vinculin
pERK(Thr202/Tyr204) levels (Normalized to ERK)
Stimulation time (min.)
D
10μg of αCD3 24h
Taok3 +/+
Taok3 +/-
Taok3 -/-
kDa
pNF-κBp65(Ser356)
NF-κBp65
Taok3
Total protein
pNF-κBp65(Ser536)levels (Normalized to NF-κBp65)
E
Taok3+/+
Taok3−/−
CD3 (μg/mL, 24h.) 0.25 0.5 1 2 5 10 20 0.25 0.5 1 2 5 10 20
pNF-κB p65 (Ser536)
NF-κB p65
Taok3
Total Protein
pNF-κB p65(Ser536)levels (Normalized to NF-κBp65)
Anti-CD3 (μg/mL)

Fig. S3. Investigation of MAPK signaling events related to TAOK3. (**A**) Immunoblot analysis of phosphorylated (p) and total JNK and P38 and TAOK3 in HEK293T/17 cells transiently transfected with vectors encoding wild-type or mutant TAOK3 for 24 hours. Total protein is used as the loading control. Densitometric analysis of amounts of phosphorylated JNK (Thr^{185}/Tyr^{185}) and P38 (Thr^{180}/Tyr^{182}) were normalized to total JNK and total P38, respectively (**B**) Immunoblot analysis of phosphorylated and total JNK, P38, and Taok3 in total mouse $CD4^+$ T cells stimulated with CD3 and CD28 for 15 minutes or left unstimulated (0). Densitometric analysis of amounts of phosphorylated JNK (Thr^{185}/Tyr^{185}) and P38 (Thr^{180}/Tyr^{182}) were normalized to total JNK and total P38, respectively. **(C)** Immunoblot analysis of phosphorylated and total ERK and Taok3 in total mouse $CD4^+$ T cells stimulated with CD3 and CD28 for 15, 30 minutes or left unstimulated (0). Vinculin is used as the loading control. Densitometric analysis of levels of phosphorylated ERK (Thr^{202}/Tyr^{204}) normalized to total ERK (**D**) Immunoblot analysis of phosphorylated NF-κB (Ser^{536}), total NF-κB, and Taok3 in the different genotypes at 10µg/mL of CD3 antibody. Densitometric analysis of amounts of phosphorylated NF-κB Ser^{536} were normalized to total NF-Kb. (**E**) Immunoblot analysis of phosphorylated NF-κB (Ser^{536}), total NF-κB, and Taok3 in a range of concentrations of CD3 antibody. Densitometric analysis of amounts of phosphorylated NF-κB (Ser^{536}) normalized to total NF-κB. Error bars represent mean ± SEM. Black dots represent biological replicates (independent experiments). Data pooled from at least three independent experiments. Statistical analysis: (A and D) One-way ANOVA and Dunnett's multiple comparisons, (B, C, E) Two-way ANOVA and Šidák's multiple comparisons tests. *$p \leq 0.05$, **$p \leq 0.01$, ***$p \leq 0.001$, ****$p \leq 0.000$.

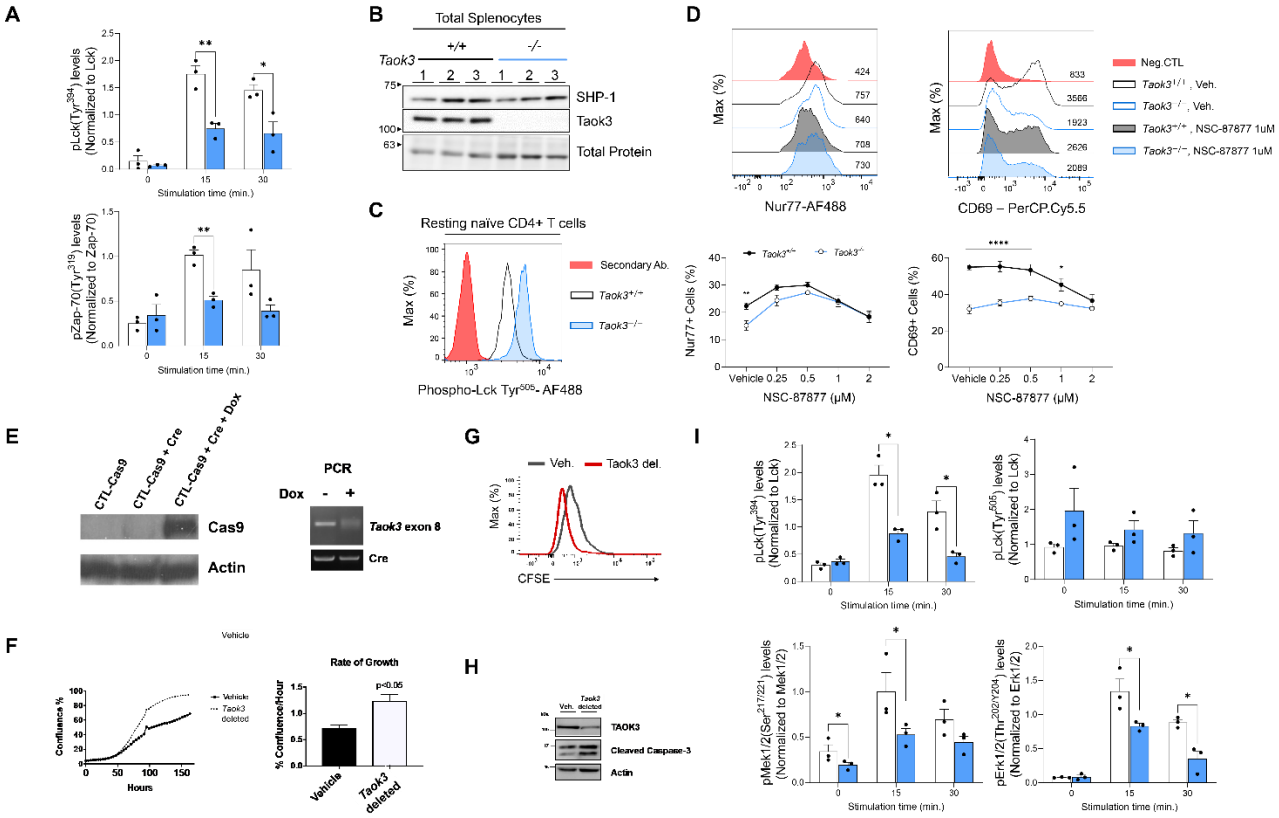

Fig. S4. Additional data relating to Fig. 4. (**A**) Densitometric analysis of phosphorylated Lck (Tyr^{394}) and phosphorylated Zap-70 (Tyr^{319}) normalized to total Lck and total Zap-70, respectively (from Fig. 4A). **(B)** Immunoblot analysis of SHP-1 and Taok3 amounts in total splenocytes. Numbers above the lanes indicate an individual mouse in each group. Total protein is used as the loading control. (**C**) Flow cytometric analysis of phosphorylated Lck (Tyr^{505}) in resting, isolated naïve CD4^{+} T cells. (**D**) Flow cytometric analysis of Nur77^{+} cells, CD69^{+} cells from Fig. 5G. Plots show the percentages of Nur77^{+} and CD69^{+} cells upon stimulation with CD3 and CD28 and treatment with the indicated concentrations of NSC-87877. (**E** to **H**) Additional results pertaining to T cells isolated from iCRISPR-Cd4-cre mouse model and treated with or without doxycycline to induce *Taok3* deletion. Immunoblot analysis of Cas-9 and PCR reaction on isolated genomic DNA from isolated T cells, treated with or without doxycycline (E). Actin is used as the loading control for the blot. Cre is the positive control for PCR. Confluency curves and growth rates (F), flow cytometric analysis of CFSE intensity (G), and immunoblot analysis of Taok3 and Cleaved Caspase-3 (H) in isolated T cells treated in culture with or without doxycycline (non-TCR stimulated). **(I)** Densitometric analysis of phosphorylated Lck (Tyr^{394}), Lck (Tyr^{505}), Mek1/2(Ser$^{217/221}$), and Erk1/2 (Thr^{202}/Tyr^{204}) normalized to their respective total protein (from Fig. 4I). Data pooled from least three independent experiments or biological replicates (mice). Error bars represent mean ± SEM. Statistical analysis: (A, D, I) Two-way ANOVA and Šidák's multiple comparisons; (F) Paired T-test. *p≤0.05, **p≤0.01, ***p≤0.001, ****p≤0.000.

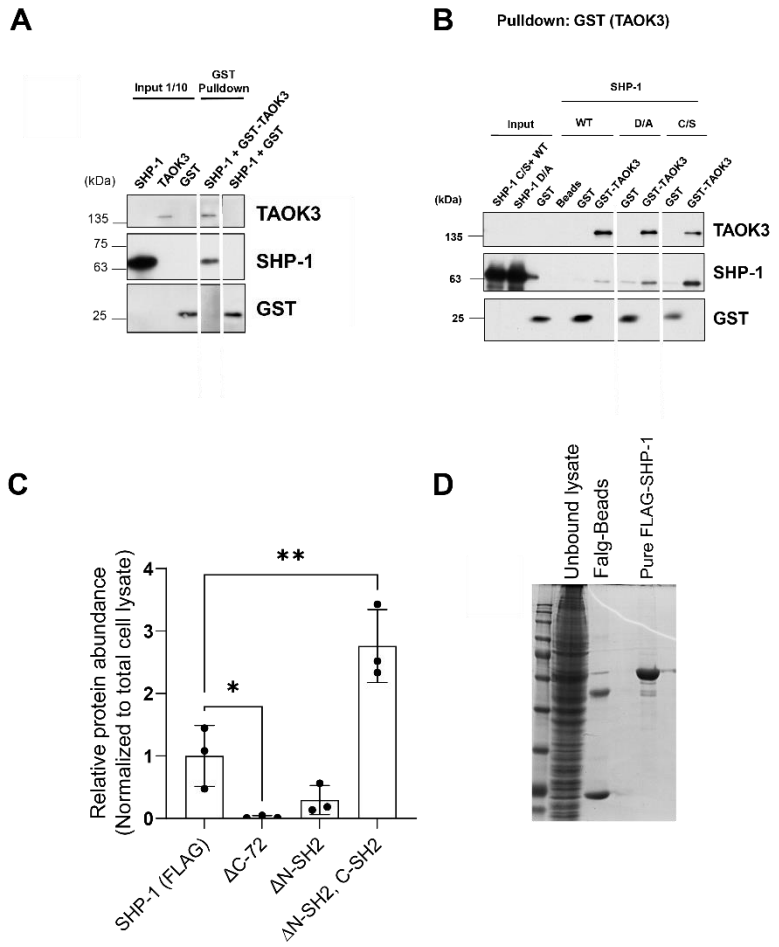

Fig. S5. Additional data relating to Fig. 5. (**A**) Immunoblotting for TAOK3, SHP-1, and GST in total cell lysates (Input) and GST pulldowns from bacterial cells (DH5α)expressing the indicated proteins. (**B**) Immunoblotting for TAOK3, SHP-1, and GST in total cell lysates and GST pulldowns from competent bacteria (DH5α) expressing the indicated combinations of WT or D/A and C/S mutant forms of SHP-1 and GST or full-length GST-TAOK3. **(C)** Densitometric analysis of the abundance of FLAG-tagged SHP-1 mutants immunoprecipitated with TAOK3 normalized to their respective abundance in total cell lysate and relative to SHP-1-FLAG. (**D**) Coomassie blue staining assessing the purification of FLAG-SHP1 from HEK293T/17 cells to be used in kinase reactions and mass spectrometry. (A, B, D) Data representative of at least three independent experiments. (C) Data pooled from three independent experiments. Black dots represent biological replicates (Independent experiments). Error bars represent mean ± SEM. Statistical analysis: (C) One-way ANOVA with Dunnett's multiple comparisons. *p≤0.05, **p≤0.01, ***p≤0.001, ****p≤0.000.

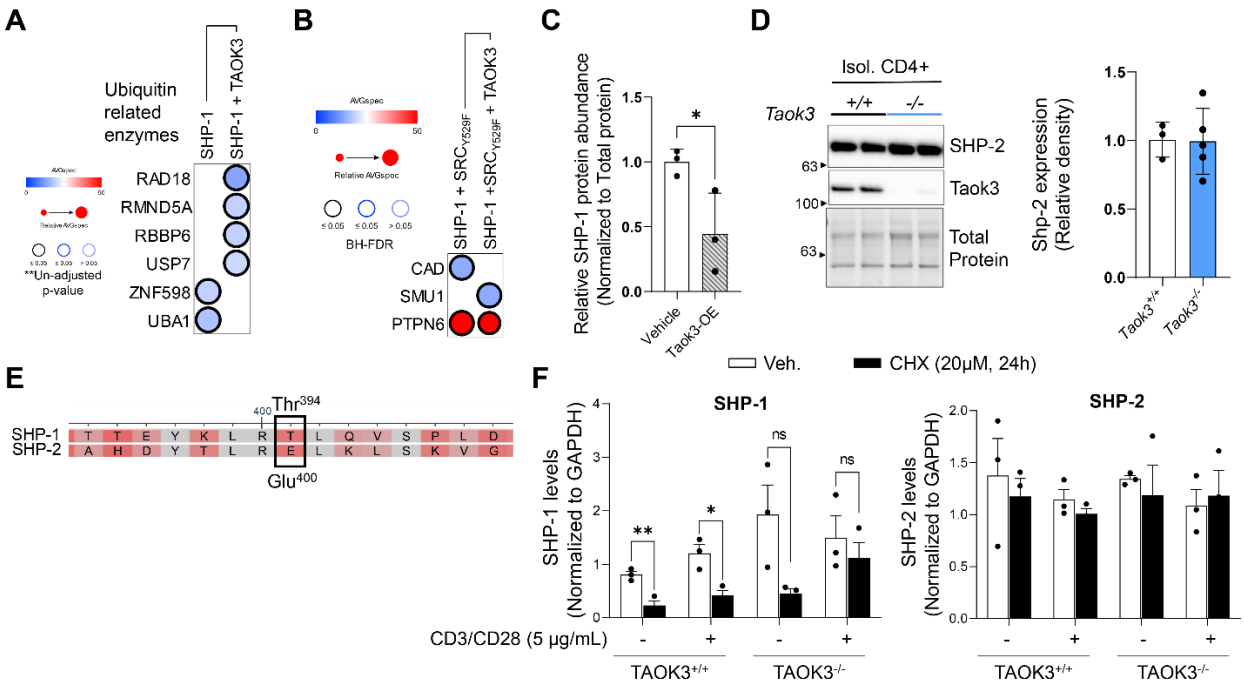

Fig. S6. Additional data relating to Fig. 6. (**A**) Ubiquitin-related enzymes found in AP-MS experiment before the adjustment of p-values. (**B**) Comparison of the enrichment profiles between SHP-1 + SRC^{Y527F} with or without cotransfection with TAOK3. Here, statistical comparison and reported FDR comparing SHP-1 + SRC Y527F versus SHP-1 + SRC Y527F + TAOK3. Differences in phosphorylated peptides abundance between SHP-1 + SRC Y527F and SHP-1 + SRC Y527F + TAOK3. **(C)** Densitometric analysis of SHP-1 protein abundance in Jurkat cells treated with doxycycline to induce TAOK3 overexpression (OE) normalized to total protein and relative to SHP-1 in vehicle-treated cells (from Fig. 6E). **(D)** Immunoblotting for SHP-2 in isolated murine $CD4^+$ T cells from either *Taok3*$^{+/+}$ or *Taok3*$^{-/-}$ animals. Total protein is used as loading control. Bar plot shows SHP-2 abundance relative to the loading control. Black dots represent biological replicates (mice). (**E**) sequence alignment between human SHP-1 and SHP-2 around SHP-1-Thr^{394}. (**F**) Densitometric analysis of SHP-1 and SHP-2 abundance normalized to GAPDH (from Fig. 6H) in *TAOK3*$^{+/+}$ and *TAOK3*$^{-/-}$ Jurkat cells. (D) Data pooled from *Taok3*$^{+/+}$ n=3 and *Taok3*$^{-/-}$ n=5 mice. (C and F) Data pooled from three independent experiments. Black dots represent biological replicates (mice or independent experiments). Error bars represent mean ± from. Statistical analysis: (D and E) Unpaired T-test, (F) Multiple unpaired T-tests. *p≤0.05, **p≤0.01, ***p≤0.001, ****p≤0.000.